This manuscript is the first version of a preprint submitted to EarthArXiv in April 2021, as such **it has not been peer-reviewed**. This contribution is to be submitted to a scientific journal for peer-review.

Authors encourage downloading the latest manuscript version from Earth ArXiv before usage.

Authors welcome comments, feedback and discussions anytime. Please, feel free to contact the first author at emmanuel.roquette@manchester.ac.uk

Integrated multi-proxy source-to-sink analysis of the Lower Cretaceous of the Essaouira-Agadir Basin.

Emmanuel Roquette [1][2]*, James Lovell Kennedy [1][2], Leonardo Muniz Pichel [3], Stefan Schröder [1][2], Rémi Charton [1][4], Ian Millar [5], Jonathan Redfern [1][2]

[1] North Africa Research Group (NARG), University of Manchester, UK

[2] School of Earth and Environmental Sciences, The University of Manchester, UK

[3] Department of Earth Science, University of Bergen, NO

[4] Department of Geoscience and Engineering, Delft University of Technology, NL

[5] British Geological Survey (BGS), UK

* Corresponding author: emmanuel.roquette@manchester.ac.uk

1.1 Abstract

This study investigates the Provenance of the Barremian-Aptian fluvial clastics exposed in the Essaouira-Agadir Basin which bears an important potential in terms of offshore feeding of reservoir sands. Thin section petrography and SEM, heavy minerals analysis, and detrital zircon dating were conducted and integrated with a large dataset of published low-temperature thermochronology studies to model the associated source-to-sink system. The homogeneity of fingerprints throughout the basin indicated a single provenance for both the northern and southern studied transects. The hinterland analysis based on LTT data revealed that only the Western Meseta and MAM regions were possible source candidates for the Barremian Aptian which was confirmed by detrital zircon geochronology. Heavy mineral populations confirmed that sediment sources were of recycled nature and rock fragment populations in the EAB revealed clasts of limestones, sandstones and volcanic nature only matching with the MAM. The Barremian-Aptian fluvial being sourced from a source-to-sink system of moderate size (200-300 km long) with an exclusive or dominant source located in the MAM (western High Atlas) provides the best fit explanation matching with each individual dataset. This likely provided a sand-rich mix of sediment resulting from the erosion of Triassic continental basins, with associated clays resulting from the weathering of basalts and Triassic /Jurassic mudstones.

Associated low sea level allowed the direct sediment supply within the slope/offshore domain where seismic imaging suggests the presence of synchronous high reflectivity deep-water channels located in structural lows controlled by diapiric salt movement. An overall NNW drainage deflection is observed offshore the northern part of the basin. The Mesetian domain is likely to be undergoing denudation at the same time and shedding a clastic-rich sediment supply north of the studied region. Due to the offshore NNW deflection of the sediment supply along the northern part of the EAB, mixing between MAM and Mesetian sands is likely offshore Essaouira making the probability of good reservoir sands in the region high.

Keywords: source-to-sink; provenance analysis; Bouzergoun formation; Lower Cretaceous; Morocco; Essaouira Agadir Basin; detrital zircon geochronology; palaeogeology modelling

1.2 **Introduction**

This study uses a combination of published (low-temperature thermochronology) and original (petrography, SEM, heavy mineral and detrital zircon geochronology) data to constrain the geodynamics of the Essaouira-Agadir Basin and its hinterland during the Barremian-Aptian. This aims to correlate probable sources of sediment in the hinterland to evaluate the origin of sands being shed to the offshore basin, with implications on reservoir prospectivity.

Reconstructing the depositional and post-depositional history of Cretaceous and older sediments within the Essaouira Agadir Basin (EAB) and its hinterland is complex. The Cenozoic Atlasic orogeny eroded large areas of the hinterland and transformed the palaeotopography and drainage systems. Within the mudstone-dominated Lower Cretaceous succession of interest, exposed in the onshore EAB, recent studies have identified a forced regression associated with an important clastic interval, dated to the Barremian-Aptian interval. This regression is thought to have been accompanied by a shift of the shoreline to the shelf edge, allowing for potential direct delivery of clastic sediments into the deep-water basin.

Understanding the timing and location of clastic delivery to the deep basin has important applied implication for reservoir prospectivity. The offshore petroleum systems in Morocco remain vastly understudied, with only 10 wells drilled in the deep-water section of the EAB. None of the wells have encountered economically viable reservoirs, although only 3 have penetrated a full Lower Cretaceous section. In Nova-Scotia, the conjugate margin of Morocco, the Jurassic and Cretaceous stratigraphy hosts large reservoirs of oil and gas. The main play is located in the Tithonian-Barremian Mississauga Fm., and Logan Fm. (Cummings, 2004; DeSilva, 1999; Neumaier, 2015). The Mississauga Fm. deposited with a progradation of the shelf margin, recording storm dominated deltaic sandstones, which are interpreted to contain half of the discovered in-place gas reserves of offshore Nova-Scotia (Cummings, 2004).

The geometry, and consequently seismic imaging of the Jurassic and Cretaceous deepwater intervals in Morocco, is complicated by salt deformation and, in places, development of allochthonous salt sheets. A key factor in any exploration is knowing where to look for the reservoirs, both in terms of temporal and spatial distribution within the basin, and an assessment of sediment type, all of which are addressed in this study.

1.3   Geological settings

1.3.1   The Essaouira-Agadir Basin

The Essaouira Agadir Basin (EAB) is located on the margin of the Moroccan shelf, at the junction of the western High-Atlas Rift Basin and the Atlantic Margin. The rifting of the Central Atlantic occurred from the Middle Triassic to the Lower Jurassic (Figure 1). Triassic syn-rift continental red beds and evaporites (Beauchamp, 1988) are followed by passive margin shallow marine carbonates of Jurassic age (Adams, 1979; Frizon de Lamotte et al., 2008). Gradual deepening occurred between the Tithonian and early Albian (Butt, 1982; Nouidar and Chellai, 2000; Rey et al., 1986), with the transition from shallow to deep shelf deposits (Figure 1).
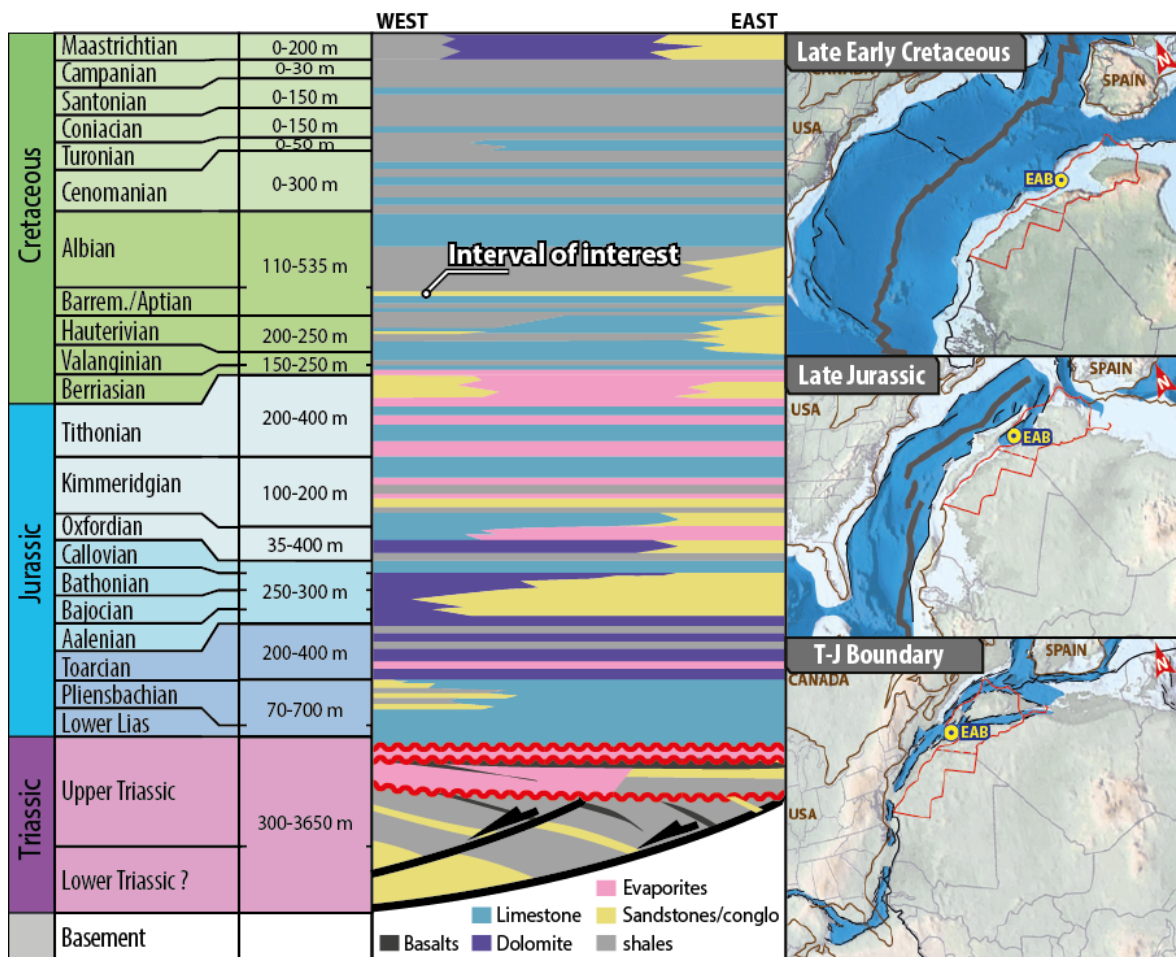

Figure 1: Regional stratigraphic chart of the onshore Essaouira-Agadir Basin, modified from Frizon de Lamotte et al. 2008 and Triassic/Cretaceous tectonic evolution of the Central Atlantic, modified from reconstructions of PALEOMAP project (Scotese, 2016).

During the Lower Cretaceous, the EAB is commonly referred to as the "Atlasic Gulf" (Behrens et al., 1978; Rey et al., 1988, 1986). The gulf formed at the connection between the High Atlas rift and the Atlantic Margin and was open to the ocean in the west (Figures 1 & 2). Its main depocenter was located close to the city of Agadir (Rey et al., 1988). At that time, the EAB formed a shallowly dipping shelf, which inherited its palaeotopography from the underlying Upper Jurassic to Lowermost Cretaceous carbonate ramp (Berriasian) (Luber, 2017).
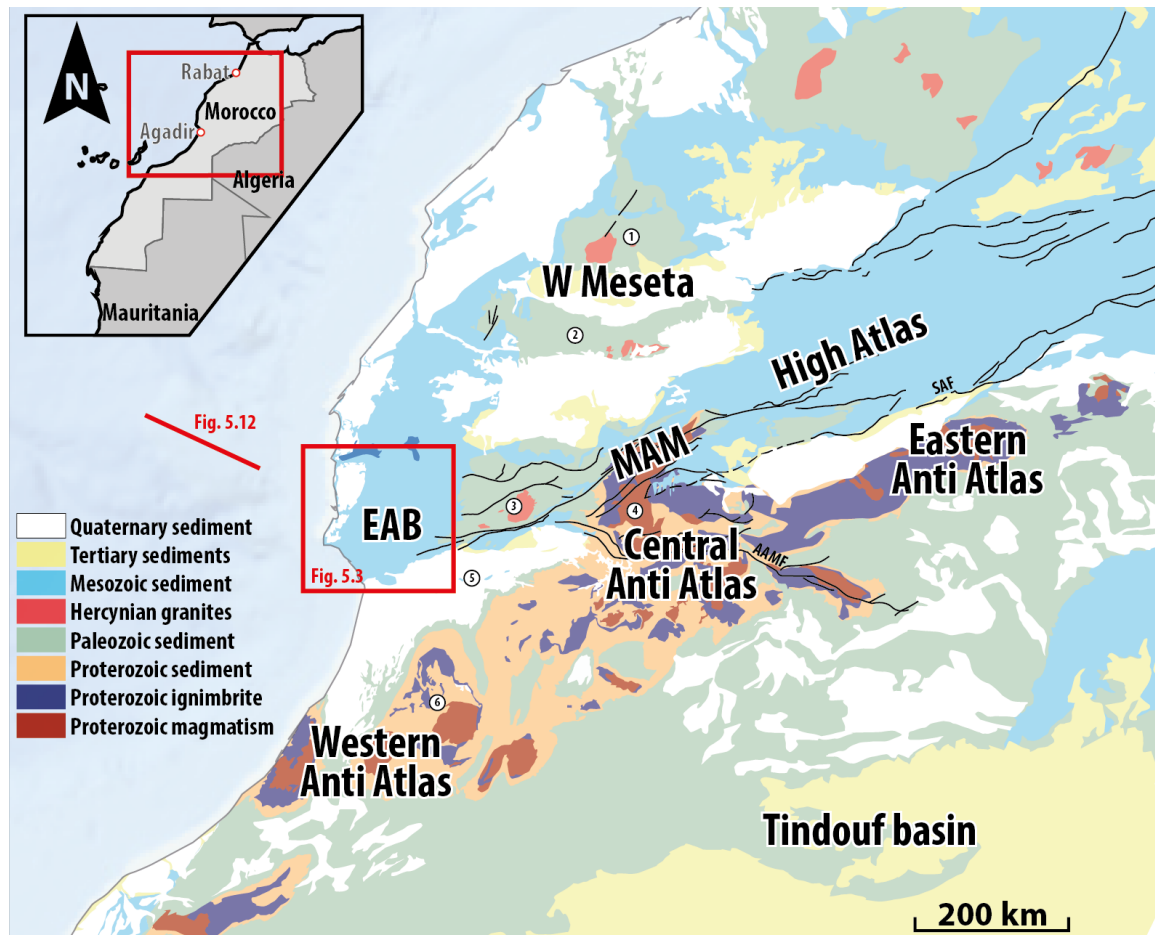

Figure 2: Simplified geological map of the hinterland of the Essaouira Agadir Basin (EAB) (modified from Saadi et al., 1985). 1: Rehamna, 2: Jebilet, 3: Tichka Massif, 4: Siroua, 5: Souss Basin, 6: Kerdous massif, SAF: South Atlas Front, AAMF: Anti-Atlas Major Front.

The Lower Cretaceous section is dominated by mudstones and minor intervals of sandstone (Luber, 2017), and displays a significant reduction in carbonate production compared to the Jurassic (Wiedmann et al., 1978). Within the Atlasic Gulf the Lower Cretaceous stratigraphy thickens towards the open ocean to the west and thins towards the continent to the east (Rey et al., 1988). Significant thickness reductions are also recognized close to salt diapir structures (e.g., Tidzi diapir) and pre-

existing, palaeo-topographic features (e.g., Cap Ghir and Jbel Amsittene, previously reported by Rey et al., 1986, 1988).

Offshore, the EAB is characterised by syn-rift Triassic fluvio-continental and Late-Triassic evaporitic series covered by a c. 6-7.5 km (c. 5-6 s TWT) Meso-Cenozoic thick overburden (Pichel et al., 2019). Salt movement was coeval with Mesozoic sedimentation leading to intense deformation of the stratigraphic secession with formation of 4-5 km tall diapirs and mini-basins as well as toe-fold-thrust systems and canopy complexes (Pichel et al., 2019; Tari et al., 2014).

1.3.2 Barremian-Aptian Regression

Within the mudstone-dominated Lower Cretaceous succession, an important phase of clastic input occurred between the Barremian to Lowermost Aptian (Luber et al., 2019) (Figure 3). This interval is part of the Bouzergoun Formation, well exposed onshore and composed of marginal-littoral sandstones, vari-coloured mudstones, dolomites, and interbedded limestone (Rey et al. 1986). This prominent siliciclastic interval is interpreted as recording a forced regression during which the shoreline shifted toward the shelf-edge, likely reaching it north of the Cap Ghir palaeo-high, and potentially delivering coarse siliciclastics directly to the deepwater basin (Luber, 2017) (Figure 3). This makes the Barremian-Aptian interval the most favourable candidate for direct clastic delivery to the deep-water basin in the Lower Cretaceous.

The Barremian Aptian regression forms the upper part of the Bouzergoun Fm. which transitions from shelfal muds with minor sandstones to shallow-marine, deltaic and fluvial sand-rich deposits. In places, erosional channels and valley features are in-filled. Palaeocurrent measurements presented on Figures 3.B & 4 were acquired by Luber 2017 from sole markings at the base of mouth bar deposits and symmetric wave-ripples. The data suggests an overall western to southwestern orientation of fluvial systems and a north-south orientation of the shoreline during the Barremian-Aptian.
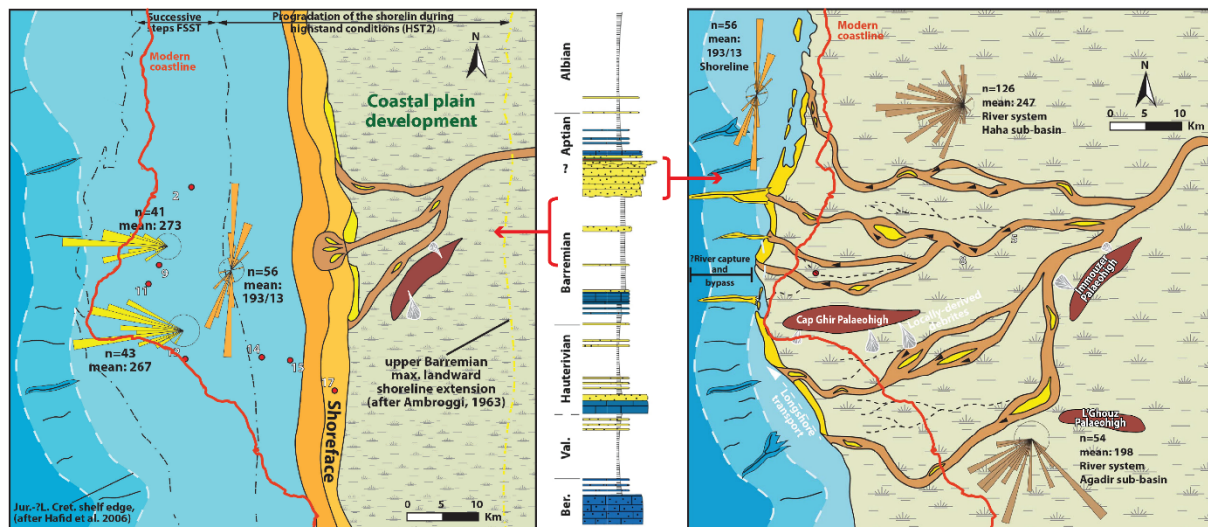
Figure 3: (A) Barremian HST2 highstand and (B) Barremian to Lower Aptian regression, red-line=modern shoreline, modified from Luber (2017), shelf edge from (Hafid et al., 2006*).

1.3.3 Hinterland domains and potential sources

The EAB is bordered to the North by the western Meseta, to the south by the Souss Basin and Anti-Atlas and to the east by the Massif-Ancien de Marrakech (or MAM, westernmost High Atlas) (Behrens et al., 1978; Luber et al., 2017) (Figure 2).

Recent studies have documented major exhumation events in all these areas during the Middle Jurassic to Early Cretaceous (Barbero et al., 2011, 2007; Bertotti and Gouiza, 2012; Charton et al., 2020; Ghorbal et al., 2008; Saddiqi et al., 2009). Areas between the Precambrian Reguibat Shield (located south of the Tindouf Basin) and the Meseta in the north (Figure 2) were affected by km-scale burial/exhumation events, largely contrasting with the post-rift thermal evolution expected along passive margins (Bertotti and Gouiza, 2012).

1.4 **Zircon record**

1.4.1 **Crystalline Basement**

In north west Africa, the crystalline basement forms part of the West African Craton (WAC). The WAC is divided into 3 domains separated by 2 intra-cratonic basins, from north to south, (1) the Anti-Atlas Mobile belt, (2) the Tindouf Basin, (3) the Reguibat Shield, (4) the Taoudeni Basin and (5) the Man-Leo Shield. The oldest rocks of the WAC are Archean in age, found within the Man-Leo and Reguibat Shields, which record crustal growth from 3.5-3.0 Ga as part of the Leonian and Liberian orogenic cycles (Potrel et al., 2007). The next major period of zircon formation was during the Paleoproterozoic

Eburnean-Birimian orogeny, which impacted the Reguibat Shield and formed the basement of the Anti-Atlas mobile belt (Boher et al., 1992; Gasquet et al., 2008) and the Moroccan Meseta (El Houicha et al., 2018).

There was then a significant period of tectonic quiescence with no known zircon formation within the basement of the WAC or more broadly within north-west Africa. This period, the Mesoproterozoic gap, is a diagnostic feature of the zircon record of Gondwana (Ghienne et al., 2018; Stephan et al., 2019). During the Neoproterozoic, on the northern margin of the WAC, the Anti-Atlas was involved in the Pan-African orogeny. The Pan-African orogeny led to the addition of numerous granitoids into the crust of NW Africa (Gasquet et al., 2008; Soulaimani et al., 2018). The final period of crustal growth along the North African margin was the Variscan Orogeny (Hoepffner et al., 2005). During the Variscan orogeny, Carboniferous-Permian aged granites were intruded into the Moroccan Meseta and MAM; no granites of Variscan age are known south of the South Atlas Fault (Hoepffner et al., 2006; Michard et al., 2008; Mrini et al., 1992).

In summary, the basement of the WAC has 3 possible age signals:

1. Southern WAC signal: Archean and Paleoproterozoic grains corresponding to the Leonian-Liberian Orogeny (3.5-3.0 Ga) and the Eburnean-Birimian Orogeny (2.3-1.7 Ga).

2. Northern WAC and Anti-Atlas signal: Paleoproterozoic and Neoproterozoic populations corresponding to the Eburnean-Birimian orogeny (2.3-1.7 Ga) and the Pan-African Orogeny (0.8-0.54 Ga)

3. Moroccan Meseta signal: Neoproterozoic and Palaeozoic zircon populations corresponding to the Pan-African Orogeny (0.8-0.54 Ga) and the Variscan Orogeny (0.36-0.25 Ga).

1.4.2 **Detrital record**

Due to the high stability of zircon grains through multiple sedimentary cycles (Andersen, 2005; Andersen et al., 2016; Morton, 1984), older sedimentary rocks are important potential sources of recycled zircon, especially in regions where the majority of the hinterland geology is composed of sedimentary rocks. In Morocco, the majority of zircons found in previous detrital studies have been of Pan-African in age (0.8-0.54 Ga) (Abati et al., 2010; Domènech et al., 2018), with Eburnean-aged grains forming a significant secondary population (Azdimousa et al., 2019; Marzoli et al., 2017). Alongside these major populations, Leonian-Liberian (3.5-3.0 Ga) and Neoarchean grains (2.5 Ga)

(corresponding to an Unknown Tectono-Thermal (UTT) event in the WAC (Abati et al., 2010) are a common accessory population. All these populations indicate that the ultimate source for these sediments was the WAC (Abati et al., 2010; Avigad et al., 2012; Gärtner et al., 2017). From Permian times onwards, Variscan grains also form an accessory population indicating that the Meseta and MAM were also a sediment source during the Mesozoic and Cenozoic (Perez et al., 2019).

The detrital record of Morocco also records zircon populations which span the Mesoproterozoic (1.6-1.0 Ga) (Accotto et al., 2019; Azdimousa et al., 2019; Ghienne et al., 2018), despite there being no known basement rocks in the WAC that could act as a source for zircons of this age range. Several sources have been proposed for these grains, including the Amazonian Craton Sunsás Belt (Perez et al., 2019), the Taoudeni Basin (Azdimousa et al., 2019; Gärtner et al., 2018), the Arabian-Nubian Shield or Sahara-Meta Craton (Accotto et al., 2019; Marzoli et al., 2017), or hitherto unknown Mesoproterozoic basement in NW Africa (Ghienne et al., 2018). These Mesoproterozoic zircons first appear in the Middle Cambrian (Avigad et al., 2012), becoming up to 30% of the zircons found within Hirnantian glacial deposits (Ghienne et al., 2018). They then diminish to form a significant accessory population during the upper Palaeozoic (Accotto et al., 2019) and the Mesozoic and Cenozoic (Azdimousa et al., 2019).

The dominance of Pan-African and Eburnean aged grains within the detrital record makes distinguishing between sedimentary sources difficult, however some trends can be identified.

1. Samples with no Mesoproterozoic populations are likely to have been sourced from WAC basement or Cambrian or older sediments

2. Samples with Mesoproterozoic populations, but no Carboniferous to Permian grains, are likely to have been sourced from the WAC basement or Cambrian and younger sediment.

3. Samples with Carboniferous to Permian populations must be sourced from either the Moroccan Meseta basement or the Permian to recent sediments.

4. Samples with both Mesoproterozoic and Carboniferous to Permian populations indicate sediment sourced from Palaeozoic sediments, the Meseta basement and/or Mesozoic to recent sediments.

1.5   Methods

12 outcrops where fluvial channels of the Bouzergoun Fm. (corelating with the Barremian-Aptian maximum regression) were exposed were studied across the basin. Petrography and geochemical analysis were carried out throughout the basin (Figure 4). Outcrops coordinate are provided in Table A2 of the appendix.
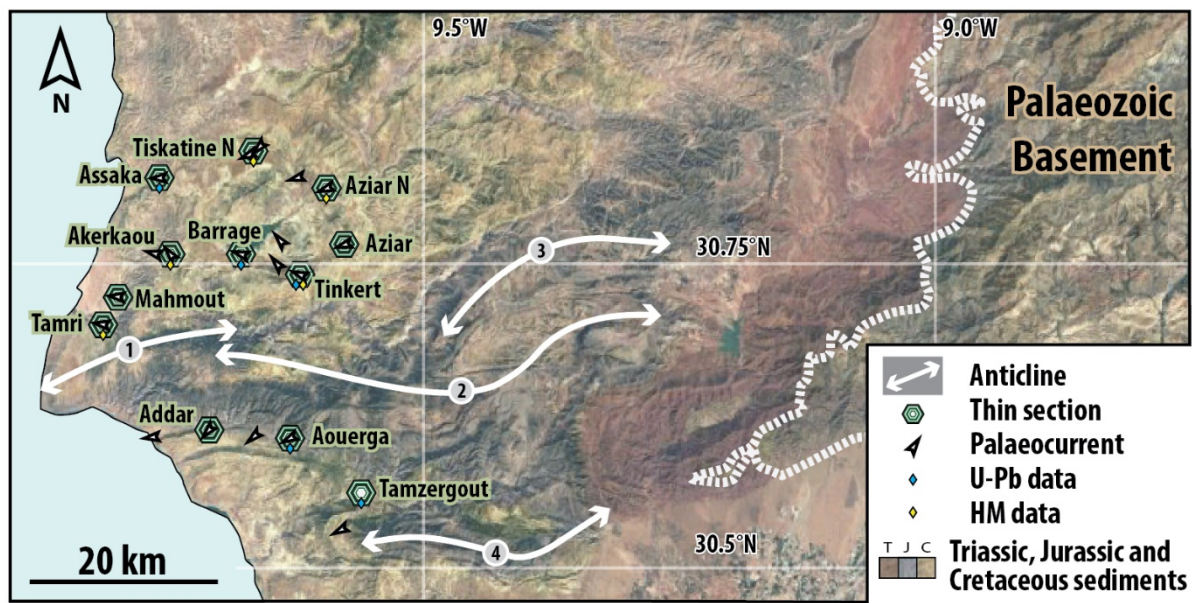

Figure 4: Overview of the Essaouira-Agadir Basin. Background: satellite picture and topography data (Google Earth© Data SIO, NOAA, U.S. Navy, NGA, GEBCO Landsat/Copernicus Data), palaeocurrents from *Luber, 2017*; 1: Cap Ghir anticline, 2: Anklout anticline, 3: Imouzzer anticline, 4: Lgouz anticline.

To be able to compare and detect variations within the basin, the outcrop data was placed into 5 groups based on geographical location : Tiskatine group (Tiskatine and Assaka sections, northern part of the basin), Tinkert group (Tinkert and Aziar sections, easternmost and most inland part of the basin), Barrage group (Barrage and Akerkaou sections, central part of the basin), Tamri group (Tamri and Mahmout sections, westernmost and most distal part of the basin) and Aouerga group (Addar, Aouerga and Tamzergout, southern part of the basin)

Thin sections were made from all sampled outcrops, they were stained for porosity and calcite and studied using optical microscopy, QEMSCAN and SEM. Thin sections were point-counted (300 points) using the Gazzi-Dickinson method (Ingersoll et al., 1984) and studied for rock fragment populations.

K-Feldspar selective staining using Sodium Cobaltinitrite (SCN), a yellow coloured salt reagent for potassium and ammonium (Bailey and Stevens, 1960), was also applied to quantify the abundance of K-Feldspar (Figure 5).However, SCN reacted with several minerals and rock fragments, which did not display polysynthetic or Carlsbad twinning, nor showed the crystal morphologies of common feldspars. Thus, additional techniques were used to determine the mineralogical composition.
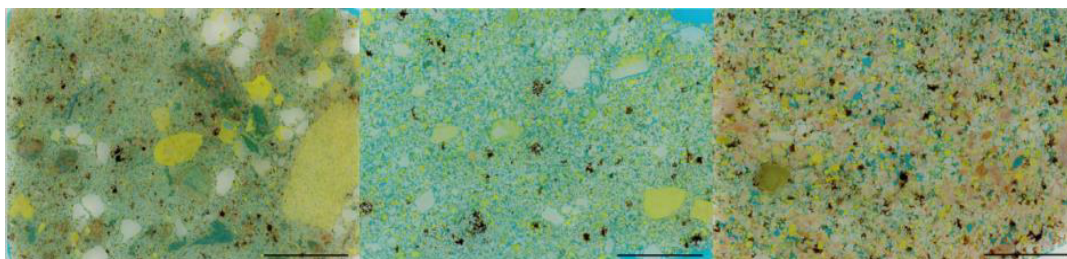

Figure 5: Thin Section overview of MTDAN 863, MTMH722 and MTTM811 (porosity in blue, SCN staining visible (in yellow) and Calcite (reddish/pink).

To help identifying the different clasts population and the nature of the sandstones, QEMSCAN (SEM based automatic mineral mapping) analysis were carried out on samples from each of the outcrops except for Tamzergout and Assaka group, which were sampled at a later stage. Cell size was set to 20 μm.

1.5.1   Heavy mineral contents

Samples were crushed using a jaw crusher. To minimize the number of broken grains, jaws were brought closer stepwise starting at a spacing of 2cm. Between each step, the product was sieved at 1mm and only the coarser fraction was re-crushed.

Samples were dry sieved at 250μm and wet sieved at 30μm. Six grams of crushed and sieved (30-250μm) samples were agitated in 25ml test tubes with 20ml of lithium heteropolytungstate (LST, density 2.86 g/cm3). Samples were left for decantation for 3 hours after which the bottom centimetre of each tube was frozen using liquid nitrogen. The bottom centimetre (heavy fraction) was recovered, mounted on glass slides, and imaged using QEMSCAN. Identified grains were then individually counted manually from the QEMSCAN maps. The QEMSCAN is unable to identified polymorphs of grains. Therefore, differentiating anatase and rutile could not be done, and both are presented together as titanium oxides.

1.5.2   Laser ablation U-Pb analysis of zircon

Five outcrops throughout the basin were selected for detrital zircon U-Pb analysis (Figure 4). For each, samples were crushed and sieved at 30-500 µm. Heavy minerals were concentrated using a shaking table and magnetic minerals were removed using a Frantz magnetic separator. Eventually, zircons were concentrated using diiodomethane (3.3 g/cm3) and concentrates were hand-picked, mounted in epoxy disks, polished, and imaged using cathodoluminescence to select laser spots. The separation, mounting and analysis of the zircon grains was conducted at the British Geological Survey (NERC Isotope Geosciences Laboratories, Keyworth). U-Pb analysis were carried out using a multicollector Nu Plasma HR mass spectrometer with a New Wave 193SS solid state laser, typically using a 20–25 µm laser spot, and fluence of c. 2 J/cm^2. Three standards (Plešovice zircon(Sláma et al., 2008), 91500 (Wiedenbeck et al., 1995), and GJ-1 (^{206}Pb/^{238}U 602.3 ± 1Ma, ^{207}Pb/^{206}Pb 609.2 ± 0.7Ma; in-house ID-TIMS) were regularly analysed to correct the instrument mass bias and depth dependent inter-element fractionation of U and Pb. The '91500' standard was used as primary throughout, yielding a weighted average ^{206}Pb/^{238}U age of 1063.9 ± 2.13 Ma (n=108). Secondary standards Plešovice and GJ-1 gave weighted average ^{206}Pb/^{238}U ages of 338.3 ± 1.0 Ma (n = 79) and 602.9 ± 1.9 Ma (n = 107) respectively. Data was reduced using Iolite (Paton et al., 2011, 2010) and plotted using IsoplotR (Vermeesch, 2018).

For grains > 1200 Ma in age, ^{207}Pb/^{206}Pb ages were used, with a discordance limit of ± 10%. For grains < 1200 Ma, ^{206}Pb/^{238}U ages were used, with a discordance limit of ± 5%. Data tables and interpretations are supplied as supplementary data and are available at following url: https://bit.ly/2Zq6nBW .

1.5.3   Hinterland analysis

The temperature history of the hinterland source areas can be ascertained from Low-Temperature Thermochronology (LTT). When reliably assessed with geological evidences, increasing temperature in a sample's thermal history is associated with burial (i.e., sedimentation above the sampled rock) and decreasing temperature with exhumation (i.e., erosion of overburden) (Figure 6). Using depth converted temperature paths, the nature of the surface geology can also be modelled. LTT datasets may record periods of sedimentation followed by periods of erosion during which the last deposited overburden is eroded. This is illustrated by the example presented on Figure 6, specifically where the area of the graph with a blue background shows a sedimentation/subsequent erosion cycle. During the first part of the cycle, sediments are deposited on top of basement rocks. When the region starts

experiencing denudation again, those sediments are gradually eroded, those deposited the latest being eroded first. Once the overburden is completely eroded, basement erosion resumes. The "ephemeral" overburden is not preserved in the modern geological record and can only be identified and reconstructed using the thermal history. Constraining these ephemeral overburdens units is critical, as a source region would, during such a cycle, be entirely or partly covered by lithologies mostly or entirely absent from the modern day known regional rock record.
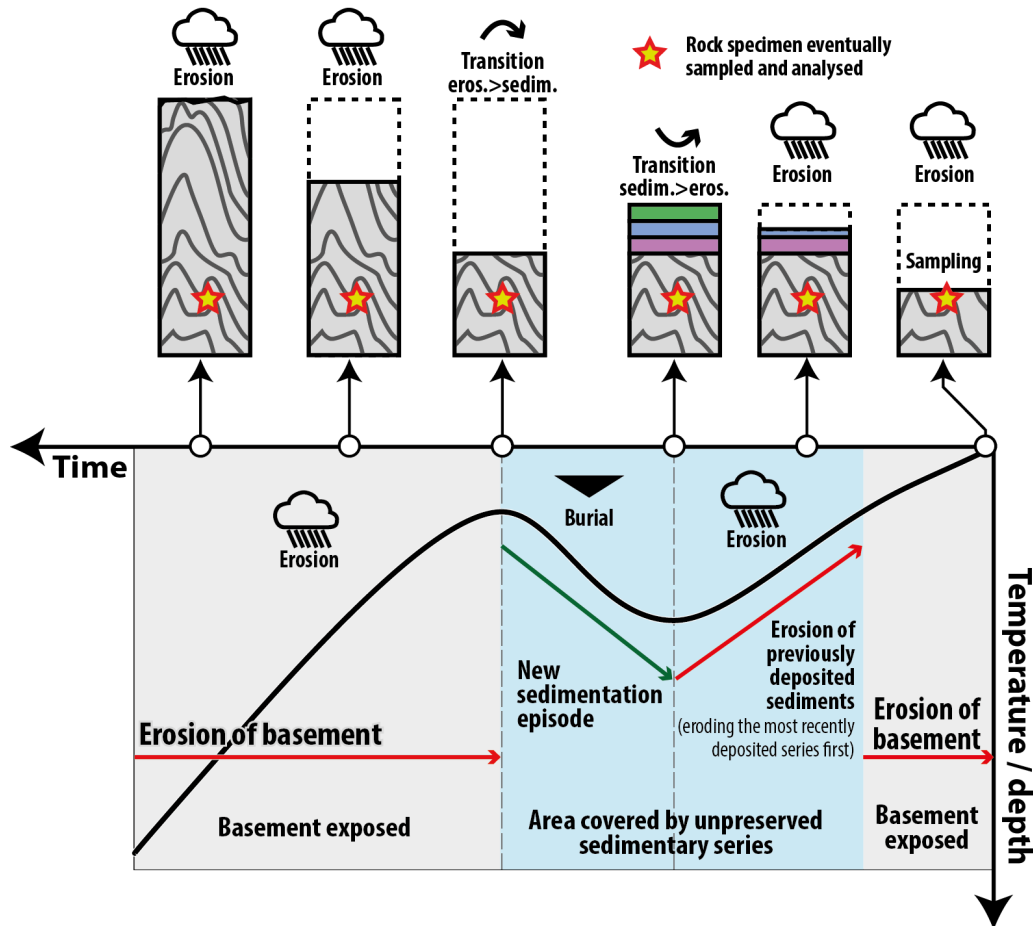

Figure 6: Burial history of a rock sample: temperature paths can be converted to depth if (1) the temperature history is only related to erosional exhumation and if (2) a consistent geothermal gradient was setup in the region. Star = rock sample eventually analysed. In this example, a subsidence/erosion cycle is marked with a blue background. During this event, sedimentation is recorded and followed by subsequent erosion. Once all the previously deposited strata are eroded, basement erosion resumes. The ephemeral sedimentary overburden is absent from the modern geology. During the time period covered by the blue background, the studied region is covered by

sediments which may have a significant influence on the surface geology and sediment supplied by erosion.

Sixteen time-Temperature models (references provided in Table A1 in the appendix A) were compiled, the slope gradient of each model was calculated at 125 Ma (Barremian-Aptian transition) and displayed on the regional map (Figure 7). Each point displays the behaviour (exhumation or burial) of the temperature path during the interval of interest.

The compilation of a large and spread-out LTT dataset allows for the location of domains undergoing erosion/sedimentation, with a focus on the Barremian-Aptian transition (125Ma) in the present contribution. Numerical modelling of time-Temperature paths is subject to large margins of error in deep times often due to a process based on a limited number of constraint points. While those error margins preclude precise time intervals interpretations of single data-points, clusters of consistent thermal history models add confidence that this reflects a regional behaviour.

1.5.4   Seismic data

We use seismic profiles from a zero-phased time-migrated dataset covering c. 2500 km^2 offshore the Essaouira-Agadir Basin. Data was provided by ONHYM and Kosmos Energy.

1.6   **Results**

1.6.1   Hinterland analysis

A large amount of thermochronology analysis conducted in the hinterland region (see Charton et al., 2020 for a summary) was reviewed and incorporated into this study. Charton et al. (2020) highlighted that all but two of the time-temperature studies compiled in his meta-analysis recorded erosional exhumation (i.e., variation of temperature being due to exhumation or burial of the rock sample). The only observed exceptions where samples from the Toubkal massif, where tectonic exhumation was the preferred scenario (Ghorbal, 2009) and samples from the Canaries where episodes of regional heating likely associated with the island formation volcanism caused the reset of parts of the fission track ages (Wipf et al., 2010). This view is consistent with other previous studies which highlighted (1) that magmatic intrusions like the CAMP dykes in the Anti-Atlas did not reset LTT ages in their vicinity (Oukassou et al., 2013) and (2) that thermal subsidence following rifting do not affect the unstretched continental crust adjacent to rift zone/rifted margins (negligible thermal relaxation) (Gallagher et al., 1998)

The behaviour of each LTT temperature path at 125 Ma is displayed on Figure 7. Compiled LTT datasets for the Barremian-Aptian transition show (1) a homogeneous cluster of data points recording denudation in the Western Meseta and MAM, (2) stable domains around the Kerdous inlier and Eastern Anti-Atlas and (3) subsidence in the central Anti-Atlas (Figure 7). Data within the Siroua region (South of the MAM) show a mix of stable and exhuming patterns. Within the Western Anti-Atlas, the signal is unclear (Figure 7).
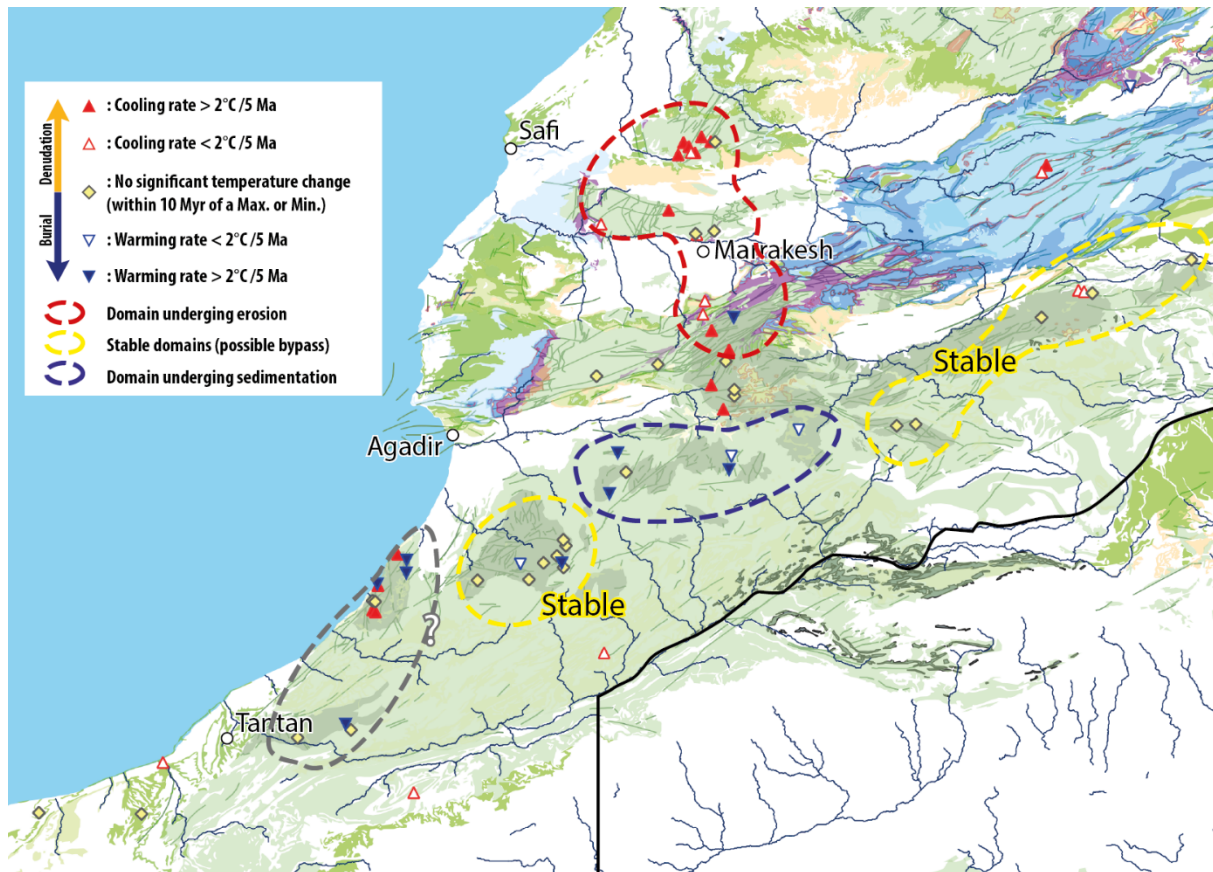

Figure 7: Temperature evolution gradient of the hinterland of the EAB at 125 Ma. The temperature dataset was assessed as recording erosional denudation (see text for details). Areas recording a decrease in temperature are undergoing exhumation (erosion) while increase of temperature highlights burial (sedimentation).

1.6.2   Petrographic analysis

1.6.2.1   Thin section petrography

All studied sections displayed litho-quartzose (7 out of 11) or neighbouring (4 out of 11) framework composition (see ternary diagram on Figure 8 based on Garzanti, 2019). Samples throughout the basin display similar rock fragment populations derived from very heterogeneous source terranes

(Figures 9 & 10). Grain size was highly variable, between and within samples, ranging from granule to fine sand. Between 9% and 29% of the point-counted samples comprise of intergranular space which may be completely cemented by calcite (e.g., Tiskatine, Addar), partially cemented (e.g., Tamri, Mahmout) or free from cement with visual porosities of up to 21% (e.g., Tinkert, Aziar South). Mono and polycrystalline quartz make up 31% to 55% of the mineralogical content. Grains are angular to sub-rounded, the sub-rounded population being highly dominant. Calcite precipitation is apparent around some of the biggest rock fragments. Detrital iron oxide and hydroxide grains are usually present and may account of up to 6% of the QEMSCAN mineral count (volumetric %), mostly consisting of goethite and hematite. The overall heavy mineral volume was estimated with QEMSCAN to be 0.2 %. QEMSCAN identified most unknown SCN-stained rock fragment as composite grains of clay, quartz, and K-feldspar. Most of these grains displayed no specific features to allow definite identification. They were included within the "rock fragment (unknown nature)" category on Figure 10.
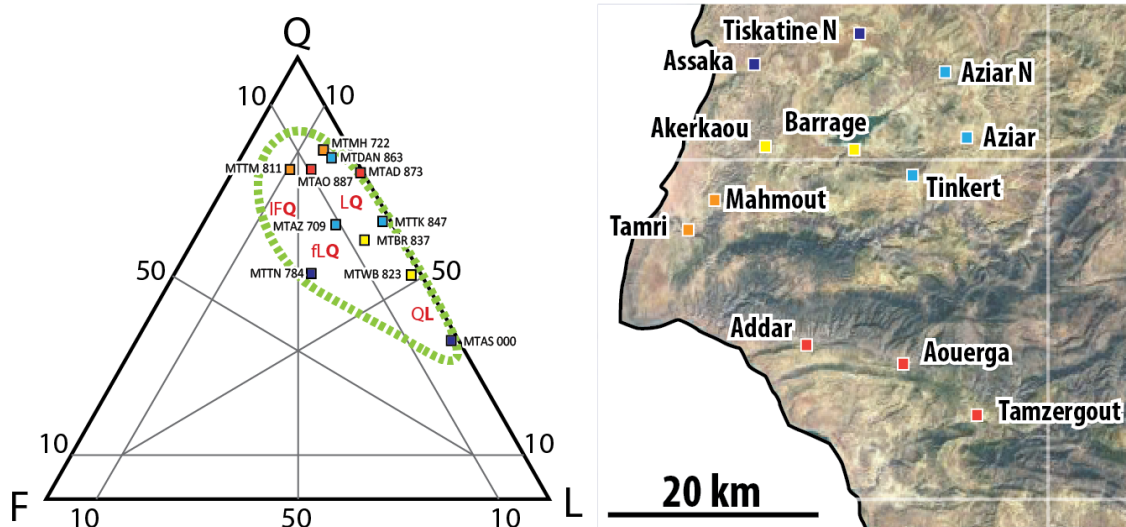

Figure 8: Sampled outcrops with analysis conducted and QFL diagram of point-counted samples (layout after Garzanti, 2019); orange = Tamri group, yellow = Barrage group, dark blue = Tiskatine group, light blue = Tinkert group, red = Aouerga group.

Throughout the basin a significant proportion of the clasts are derived from volcanic rocks (Figure 10). It included populations of pumice clasts (Figure 9D), embayed quartz, formed during igneous extrusive volcanism events and fragments displaying graphic/granophyric texture. Such intergrowth of quartz and alkali feldspar is also commonly found in volcanic clasts (e.g., ignimbrite) or shallow level felsic intrusions (Ulmer-Scholle et al., 2015). Most of these clasts were in an advanced state of

weathering and gave similar QEMSCAN signature as unidentifiable SCN-stained rock fragments. Unaltered volcanic glass is known to be isotropic but alteration to quartz or K-feldspar and SCN staining has previously been suggested to help identify the presence of what was once volcanic glass within lava, ignimbrite or pumice grains (Ulmer-Scholle et al., 2015). As volcanic grains tend to be hard to identify after weathering as they alter to clays (smectite, illite, chlorite, etc.) (Aomine and Wada, 1962; Sudo, 1954), their original abundance is thought to be larger than that assessed by point-counting (Figure 10) and was possibly an important part of the unidentified SCN-stained grains.

All samples were poor in feldspar (4.2% in average, see QFL on Figure 8). Grains identified as feldspar were in an advanced state of alteration and commonly reacted with SCN staining. Some clasts remained identifiable by displaying characteristic white perthitic worm-like structures, interpreted as albite exsolution lamellae (Figure 9C). The SCN-stained part of the grain in Figure 9C is likely made of K-Feldspar partially altered to albite and clay minerals. Pores likely formed during the weathering process and were filled by calcite or quartz cement (≈50 μm roundish/elongated structures visible in the grain). The preferential dissolution of the albite lamellae may create important porosity, up to 10% in the grain displayed in Figure 9C, speeding up weathering of the grain. Dissolution is likely to have been prominent after deposition as the observed degree of dissolution of perthite grains is incompatible with transport (Figure 9A).
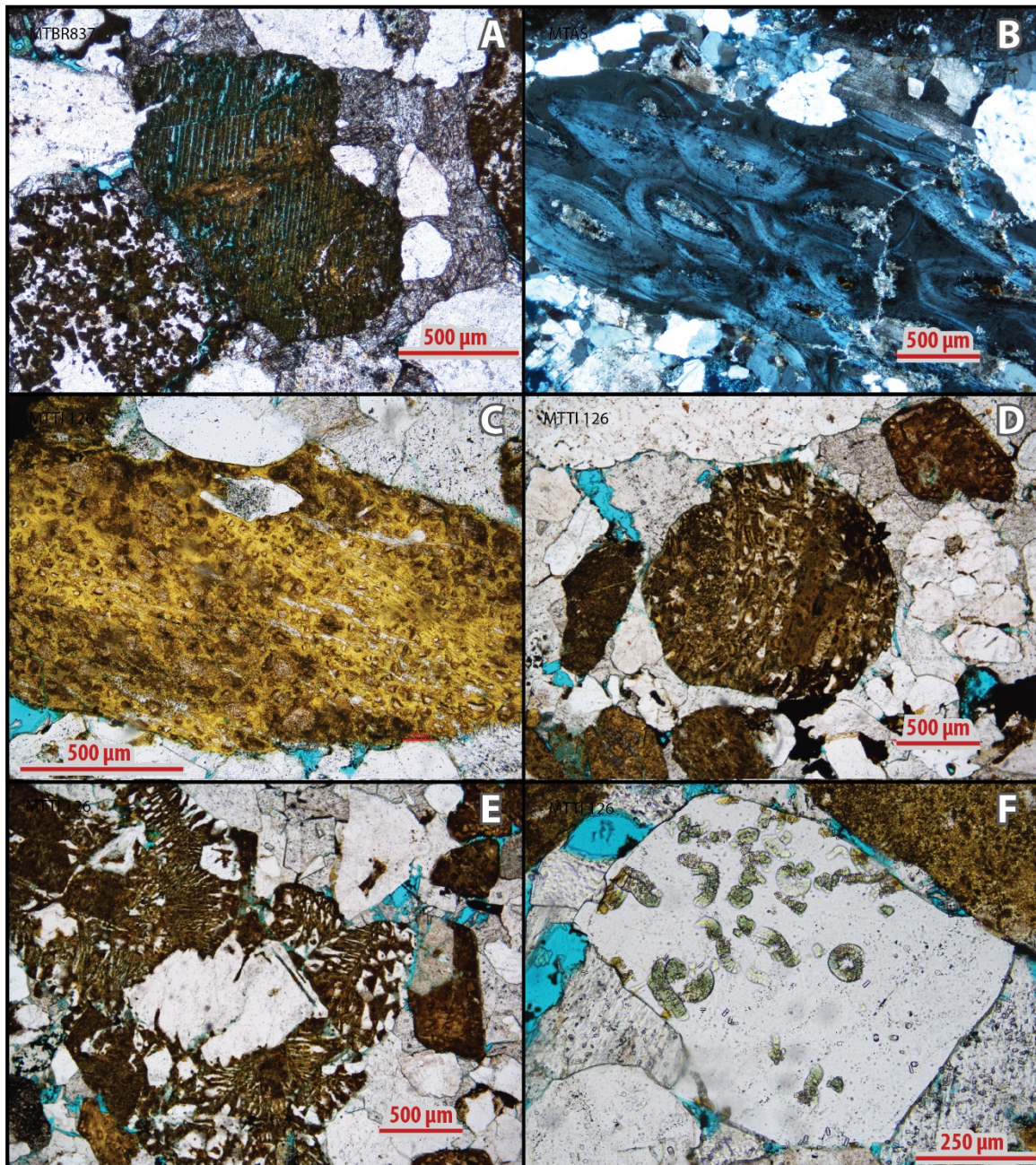
Figure 9: Microphotographs (polarised light) of clasts from : A: Perthite grain with dissolved albite lamellae, this level of dissolution is incompatible with transport and likely to be post-depositional; B: Deformed possible serpulids or ooids with pore filling carbonate cement; C: deeply weathered feldspar with exsolved albite lamellae and inclusion; D: SCN stained grain of pumice; E: Granophyric texture commonly found in volcanic terranes or shallow felsic intrusion; F: Hydrothermal chlorite inside of a Quartz grain (hydrothermal metamorphism).

1.6.2.2   Rock fragment population

All samples display an important (6-16%) population of volcanic-derived rock fragments (Figure 10). Carbonate rock fragments are also consistently present throughout the basin, especially in the Tamri group. This group is dominated by rounded to subrounded grains of calcite, with rare rounded fragment of fossil bearing limestone also present (e.g., possible serpulids, Figure 9B). Rare grains of quartz displayed vermicular chlorite inclusions (Figure 9F) typically derived from terranes subject to hydrothermal alteration (Espejo and Lopez-Gamundi, 1994) or within metamorphic or pegmatitic terrains (Ulmer-Scholle et al., 2015). Metamorphic-derived rock fragments were found throughout the basin, with the exception of the Tamri Group. All sample groups have polycrystalline quartz, differentiated based on the shape of quartz minerals within the clast as igneous and detrital origin. When the distinction between either category was unclear, grains were simply identified as polycrystalline quartz ("Qtz – Poly" on Figure 10).
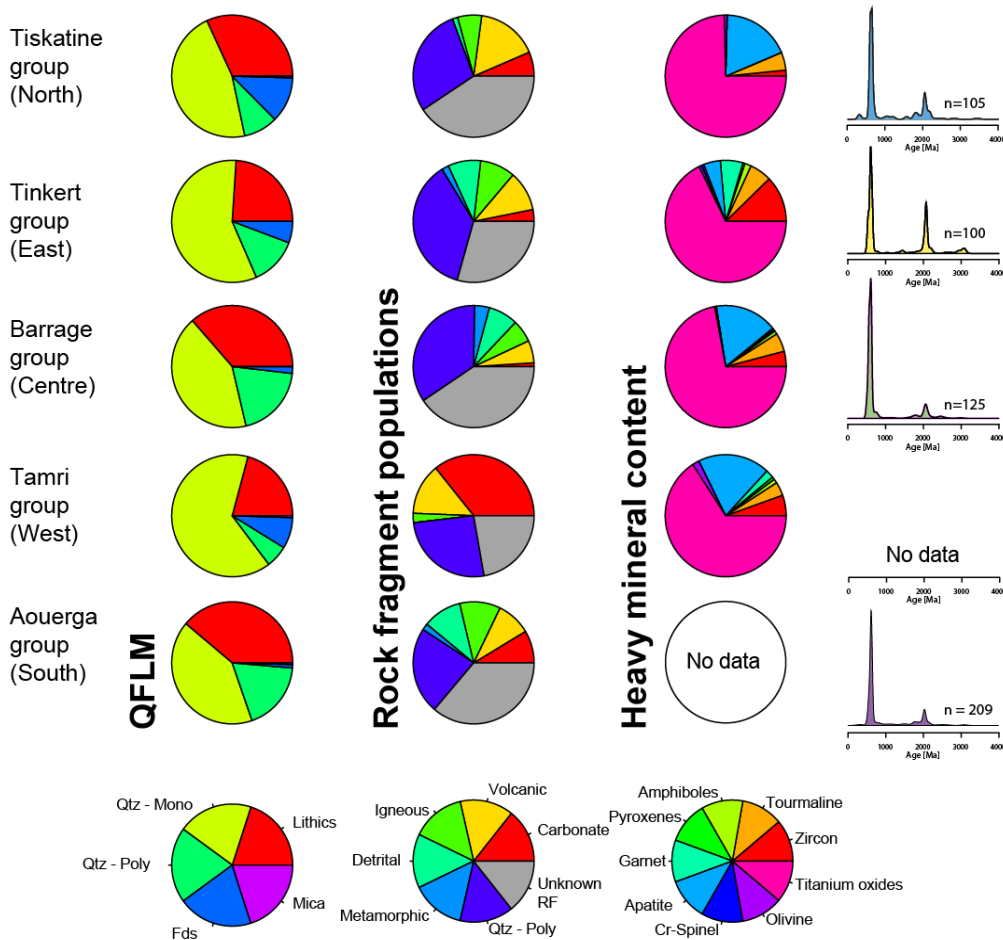

Figure 10: Modal composition, rock fragment population, heavy mineral content and detrital zircon spectrum of studied sample groups.

1.6.3 Detrital zircon dating

All samples display the characteristic northern WAC detrital zircon spectrums dominated by a major peak of Pan-African age and a secondary peak of Eburnean age (Figure 10). The Tiskatine group (north) have the most diverse assemblage of secondary populations including Variscan grains and Mesoproterozoic grains. Samples from the Aouerga group (south) have similar populations, but a single Variscan grain was also recorded. This Variscan population was not found in the Barrage and Tinkert group. All samples have at least one grain of Mesoarchean age (around 3Ga) and the Tiskatine group has the only grain in the dataset of Paleoarchean age. Mesoproterozoic grains were present as a trace population in all samples. Overall, no distinguishing populations or trends are visible between the northern and southern part of the basin.

1.6.4 Heavy minerals

Heavy mineral assemblages within a sedimentary rock are the results of various factors: lithology of the parent rocks, weathering in the source area, mechanical abrasion during transport, post-depositional weathering, hydraulic processes, diagenesis, and weathering at outcrop (Guedes et al., 2011). Samples were variably affected by dolomitization and iron oxides and had different heavy mineral yields. On sample MTTN784 from Tiskatine group, 80 to 90% of the separated heavy minerals were dolomite fragment (Figure 11) and only 126 non-dolomitic transparent heavy minerals were present in the mount. In other samples, the number of transparent heavy minerals recovered (excluding iron oxides and dolomites) varied between 222 and 312.
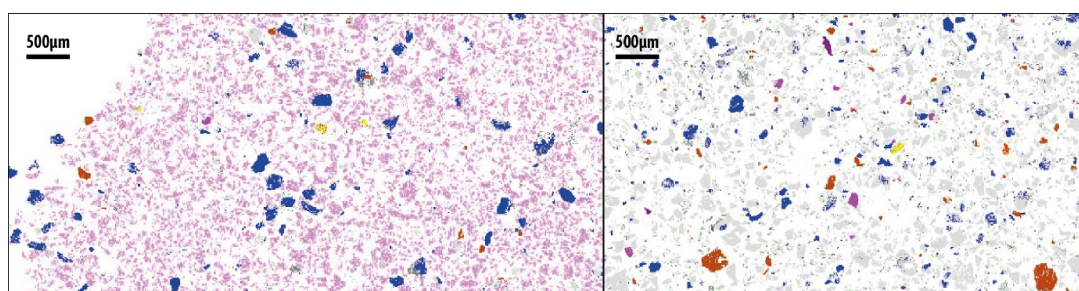

Figure 11: Overview of heavy mineral mounts from samples MTTN784 and MTTM811, dolomite in light pink and iron oxides in light grey account for most of the signal in each sample (other minerals: apatite in brown, zircon in purple, titanium oxides in blue, tourmaline in yellow).

In all samples, the heavy mineral content is dominated by ultra-stable minerals (titanium oxides, zircon and tourmaline), with ZTR ratios (Hubert, 1962) of 75 to 86%. Titanium oxide minerals largely dominate the heavy mineral mix (65 to 75% of grains) and all samples present the same secondary

population of apatite (5 to 19%). Rare olivines are also present throughout the basin (0.5 to 1.8%) (Table 1). The only compositional differences between samples are within trace populations: the Tiskatine group do not have amphibole which accounts for 0.9 to 1.7% of other groups, nor does it have pyroxenes (0.5 to 0.7% in other groups) or garnet (0.5 to 6%). Cr-spinels were only detected in the Tinkert group (4 grains, 0.7% of HM mix). Those differences among populations are represented by very small number of grains (4 or less) and may be the result of statistical effects.

	Tinkert-Aziar group (East)	Tiskatine Assaka group (North)	Tamri-Mahmoud group (West)	Barrage-Akerkaou group (Centre)
Zircon	71	2	15	9
Tourmaline	34	6	10	11
Amphiboles	10	0	3	2
Pyroxenes	3	0	2	1
Garnet	35	0	6	1
Apatite	26	23	53	37
Cr-Spinel	4	0	0	0
Olivine	4	1	5	1
TiO2	392	94	181	160

Table 1: Result of heavy mineral point counting. Conducted on QEMSCAN maps of mounted heavy mineral condensates.
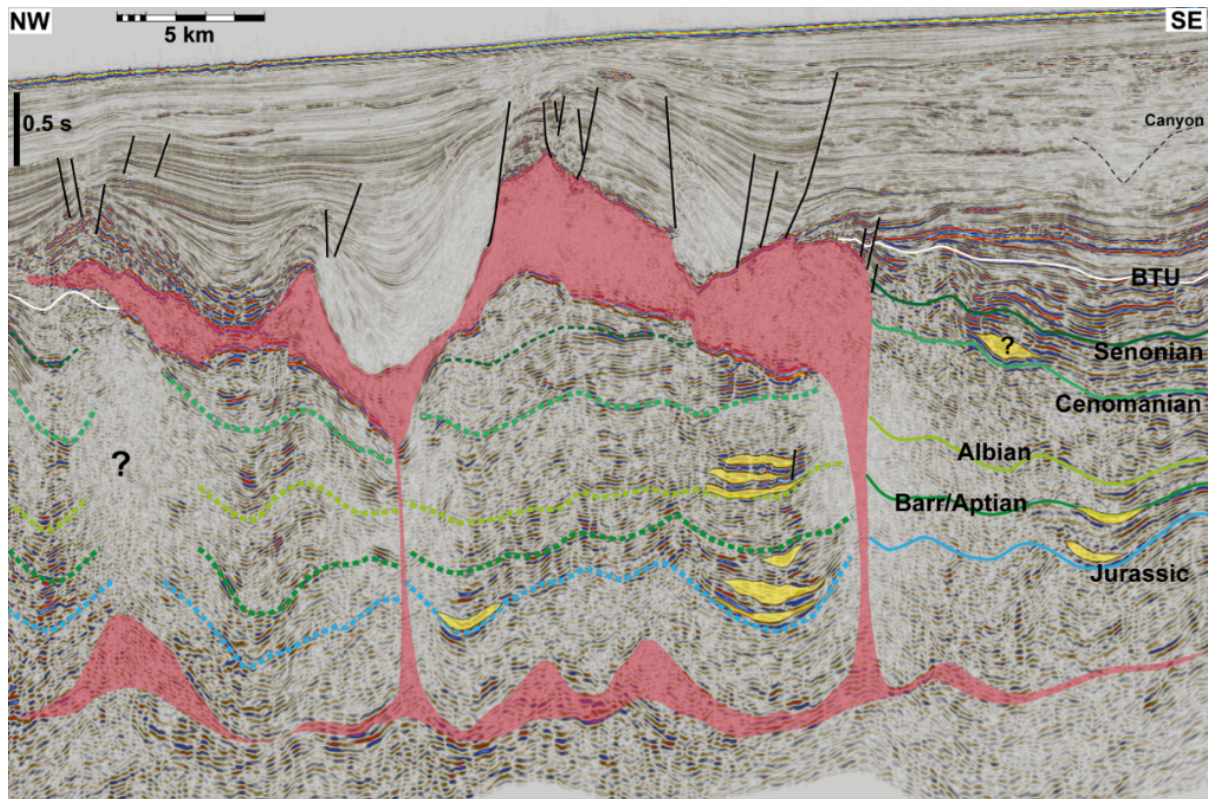
Figure 12: Interpreted seismic profile offshore Assaka. Salt canopy in red, high amplitude channel-like possible sand bodies in yellow. Uninterpreted version provided in the appendix (Figure A).

Offshore seismic profiles show indications of Barremian-Aptian, Cenomanian and, possibly Jurassic lenticular to convex-shaped mini-basins. They are characterised external geometries with internal high-amplitude seismic facies (Figure 12). These structures are located in structural lows and display onlaps towards upturned strata in the flank of diapirs and/or salt-cored anticlines. They can be confidently mapped within the two more proximal mini-basins in the mid-slope. They are continuous and can be seen on several profiles indicating a direction of sediment transport towards NNW likely due to deflection around NNW-trending diapirs (Figures 12 & 14).

1.7   Discussion

1.7.1   Areas of denudation and surface geology in the hinterland during the Barremian-Aptian

Thermochronology data shows that the MAM and Western Meseta record denudation during the Barremian-Aptian transition (Figure 7). Data within the Anti-Atlas do not show any trend of denudation. The behaviour of the Western Anti-Atlas is unclear but the dominance of east-west oriented palaeocurrent measurements in the EAB supports sourcing from the east. This excludes

sediment input coming from the Western Anti-Atlas located to the south-west but do not suffice to discriminate between the MAM and Western Meseta.

Depth-converted LTT data in the MAM and Western Meseta (Charton et al., 2020) indicates the presence of an unpreserved overburden (see method section for details) covering both regions during the Barremian-Aptian transition (Figure 13). At that time, both regions are at the end of a burial/exhumation cycle during which sediments were deposited above the Palaeozoic and Precambrian basement (Figure 13). This sediment cover over the Western Meseta was originally deposited when the region underwent burial during the Triassic to Lower Jurassic time (Figure 13). The region recorded the accumulation of 2.5 to 4 km of sediment before exhumation resumed around 180Ma. Between the onset of the exhumation phase and the Barremian-Aptian transition, a large part of the overburden was eroded and during the studied interval, the Western Meseta is expected to be covered by a few hundred meters to up to 1 km of latest Permian (in the Jebilet) to Triassic sediments, Jurassic sediments having been eroded first. Basement exposure in the Rehamna massif is possible. Lithologies within the overburden were likely dominated by continental clastic deposits as described in the Permian stratigraphy proposed by Hoepffner et al., 2005, and on preserved Permian/Triassic conglomerate and sandstones (Mader et al., 2017; Medina, 1995).

The MAM underwent burial during the Upper Triassic and throughout the Jurassic before exhumation resumed around the Jurassic-Cretaceous boundary. At that time, 3 to 4 km of sediment had deposited over the MAM. Part of it was subsequently eroded and during the studied interval, the MAM was covered by an Upper Triassic- Middle Jurassic overburden with a thickness from a few hundred meters to up to 1.6 km.
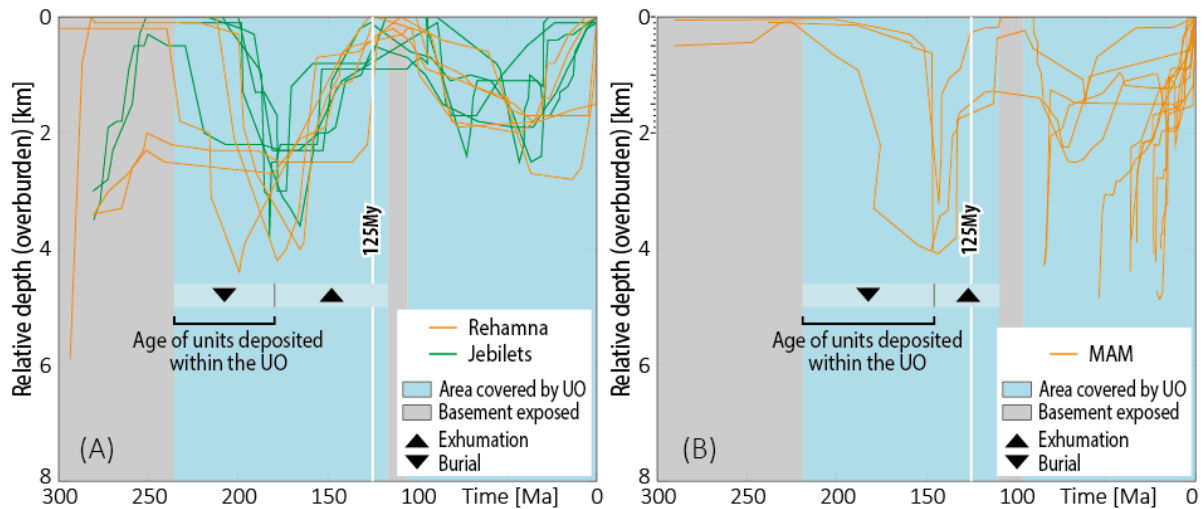
Figure 13: depth converted LTT data in the Western Meseta (A) and MAM (B), modified from Charton et al. (2020). UO = unpreserved overburden; grey background = periods of basement exposed, blue background = burial/exhumation cycle during which the studied region is covered by an overburden absent from the modern geology, see Methods for details.

1.7.2 Nature of unpreserved overburden over the WMA region

Depth converted curves indicate that the 2-4 km thick overburden over the Rehamna is mostly or entirely eroded during the Barremian-Aptian and basement exposure is likely. 100s of meter of sediment deposited during the Triassic are however still overlying the Jebilet basement. In the MAM, 1-2 km of Triassic to Middle Jurassic sediments are covering the basement terranes.

In the Lower to Upper Triassic, sedimentation within the MAM corridor, connected to the EAB, is thought to be dominated by siliciclastic deposits and associated with fine siliciclastics. This interpretation is based on remnants of Permo-Triassic sediments preserved in intra montane rift basins (Fabuel-Perez et al., 2009; Le Roy and Piqué, 2001) (e.g., Oukaimeden Basin, Tizi N Test Basin) and paleogeographic reconstructions (Beauchamp, 1988; Frizon de Lamotte et al., 2008; Medina, 1995). While Frizon de Lamotte et al. (2008) predicted the sedimentation of unpreserved conglomerate and clastics in the Western Meseta, no remnants are preserved to test the model. Those Triassic series would have transitioned laterally towards the west into an alternation of siltstones and sandstones as visible in the DA-8 well (Doukkala Basin, Le Roy and Piqué, 2001), and be capped by evaporites and basalts during the Latest Triassic/Sinemurian period (Le Roy and Piqué, 2001; Medina, 1991; Sahabi et al., 2004).

During the Triassic-Jurassic transition, extensive tholeiitic flood basalts of the Central-Atlantic magmatic province were formed around the MAM region and dated to 200 ±3 Ma (Schlische et al., 2013). The data shows the MAM was undergoing burial during the Triassic-Jurassic transition (Figure 13) and while unpreserved in the modern geology, CAMP basalts are expected to have been deposited across the MAM region with a calculated average thickness of 225 ±75 m based on surrounding regions (150m thick basalts in the Argana Basin (west of the MAM), and 300m in the Central High Atlas (Le Roy and Piqué, 2001; Marzoli et al., 2019)).

These results suggest that during the Barremian-Aptian the surface geology in the Jebilet was likely dominated by coarse clastic sediment covering most or all of the Palaeozoic basement. Erosion of the region is expected to yield good quality sands. On the other hand, Triassic sands in the MAM were partly covered by volcanic and lagoonal deposits delivering a sand-rich but more heterogeneous mix with basalt, clay, carbonate and siliciclastic rocks undergoing erosion.

1.7.3 Intra-basinal homogeneity

The integrated dataset of detrital zircon, heavy mineral and petrography points toward a similar recycled source for the different parts of the basin.

Eburnean and Pan-African peaks within detrital zircon datasets are common throughout north Africa and are too widespread to be used as a provenance indicator (all possible source terranes are susceptible of yielding such ages). The studied dataset however contains Variscan grains recorded in both the Tiskatine group (north of basin) and Aouerga group (south of basin), and therefore likely present throughout the basin. The population was probably not detected within the Tinkert and Barrage groups due to their limited sample size (respectively 100 and 125 grains).

The scarcity of feldspars and the abundance of sub rounded quartz and sedimentary rock fragments tends to indicate that source terranes are dominantly sedimentary in nature. The low heavy minerals contents estimated using QEMSCAN (0.2 % of the total mineral volume) is consistent with this interpretation and suggests reworking of a mature sediment input. The homogeneously high ZTR ratios in all analysed samples also suggest a very high degree of mineralogical maturity and may be the result of extensive recycling and/or of post depositional dissolution of less stable mineral species (Garzanti and Andò, 2007).

Heavy mineral contents are similar between samples throughout the basin with minor differences in the east (Tinkert group), which has higher proportions of zircon, tourmaline, amphibole, garnet and

is the only sample containing Cr-spinel. However, the sample also has the lowest apatite content (4.5% versus 17-19% in other groups). Apatite is known to break down easily when exposed to weathering (Morton, 2012) and the high relative values of secondary populations in the Tinkert group are likely a statistical artifact due to the loss of apatite during the post depositional weathering.

The nature and proportion of rock fragment populations is also similar throughout the basin with important carbonate, volcanic, detrital and igneous lithic fragment. The Tamri group is enriched in carbonate rock fragment and has reduced detrital and igneous rock lithic content relatively to other populations. However, the group is surrounded to the north, east and south by sections sharing a high degree of similarity together, and the peculiar fingerprint of the Tamri group is unlikely to be the result of a different regional provenance, but more likely the result of local sediment sources (possibly from the Cap Ghir palaeohigh) or the result of hydraulic sorting.

1.7.4 Provenance correlations

Samples throughout the basin contain Variscan grains only known to be sourced from Variscan igneous units or Permian and Triassic detrital terranes of the Western Meseta and MAM.

Based on the expected lithologies within the unpreserved overburdens, Triassic sediments are the most likely source of clastics to the EAB. Triassic sediments of the MAM and Argana Valley (Eastern EAB) are characterised by the presence of scarce Variscan grains and a minor but consistent population of Mesoproterozoic. Archean grain can represent a minor population (as exemplified in Marzoli et al. (2017)) in the basal Triassic (Perez et al., 2019, Domènech et al., 2018)) or a major one (Upper Triassic of Oukaimeden and Tizi N'Test (Perez et al., 2019, Domènech et al., 2018)).

Samples from the Barremian-Aptian fit perfectly in this framework (Figure 14) with grains within all expected age windows and a relative scarcity of Archean grains. The proportion of dominant and accessory zircon populations correlate with a sediment supplied at least in part from reworked Triassic sediments.

The MAM is the best candidate for the pyroxene/olivine content and volcanic lithics, likely derived from the erosion of CAMP basalts expected at the time in the region. While the Western Meseta is also thought to have been subsiding during the Triassic-Jurassic transition and therefore possibly recording CAMP volcanics, the LTT data indicate those would have been eroded before the Barremian-Aptian transition (Figure 13). During the studied interval, the MAM is also thought to be

covered by a sedimentary overburden comprising of limestones and sandstones, making it the only known match for the observed rock fragment populations in the basin.
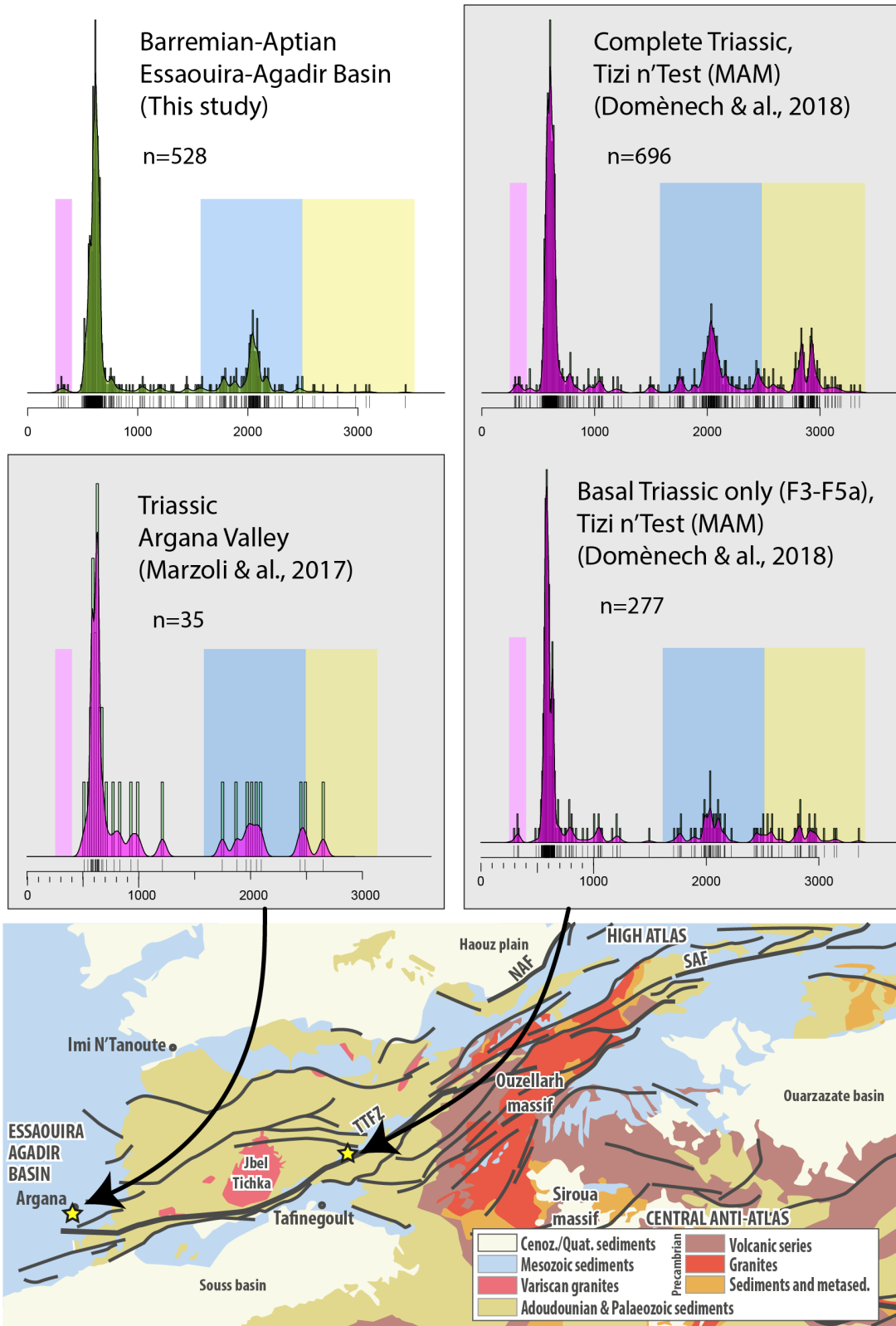
Figure 14: similitude between detrital zircon geochronology data from Triassic and Barremian-Aptian sediments (Domènech et al., 2018; Marzoli et al., 2017). Color bands: pink=Variscan, blue=Paleoproterozoic, yellow=Archean.

1.7.5 Possible contribution of the Meseta

The homogeneous fingerprints throughout the basin suggest all sections are being sourced from similar terranes, and the petrographic dataset points toward a sediment supplied in part or entirely from the MAM through an E-W local drainage. In the presence of E-W rivers coming from the MAM towards the EAB, for Mesetian sediments to reach the southern part of the basin would involve transfer perpendicular and across those rivers which do not fit with a realistic scenario. The Western Meseta (especially the Jebilet mountains) is expected to yield sand rich sediment during the studied interval and a significant clastic influx to the north of the basin would have affected the fingerprints observed in the Tiskatine group which is not visible in our dataset.

All evidence points toward a proximal source, the MAM as the dominant and possibly exclusive source of sediment of the system.

1.7.6 Nature of the sediment supply and offshore component

The LTT data indicate the region is at the end of a burial/exhumation cycle (Figure 13), layers deposited first being eroded last, the MAM is expected to have Triassic clastic basins undergoing erosion, along with the CAMP and Jurassic lagoonal deposits supplying the EAB with dissolved carbonate, sands and possible clays resulting from the weathering of volcanic/basaltic rocks and erosion of Jurassic mudstones.

The low sea-level associated with the Barremian Aptian regression allowed the migration of deltas to the shelf edge and the sediment flux was directly supplied to the slope/offshore domain (delta fed canyons). Seismic imaging suggests the presence of synchronous deep-water channels located in structural lows created following diapiric salt movement (Figure 12). Sediment transport direction was variable and following input from the shelf, it is observed oblique to the margin as sediments were being deflected and ponding behind and around rising salt walls and remained partly trapped within more proximal, mid-slope mini-basins. An overall NNW drainage direction is observed offshore the northern part of the basin (deflecting around N-NW-trending diapirs) while the southern part was not imaged and might have been feeding an early Agadir Canyon (Figure 14).

Synchronously, the Mesetian domain is likely to be undergoing denudation and shedding a clastic-rich sediment supply further north, outside of the sampled region (Figure 14). The associated river system is not preserved and the geometries of the onshore drainage pathways are unknown.

However, due to the offshore NNW deflection of the sediment supply along the northern part of the EAB, mixing between MAM and Mesetian sands is likely offshore Essaouira.
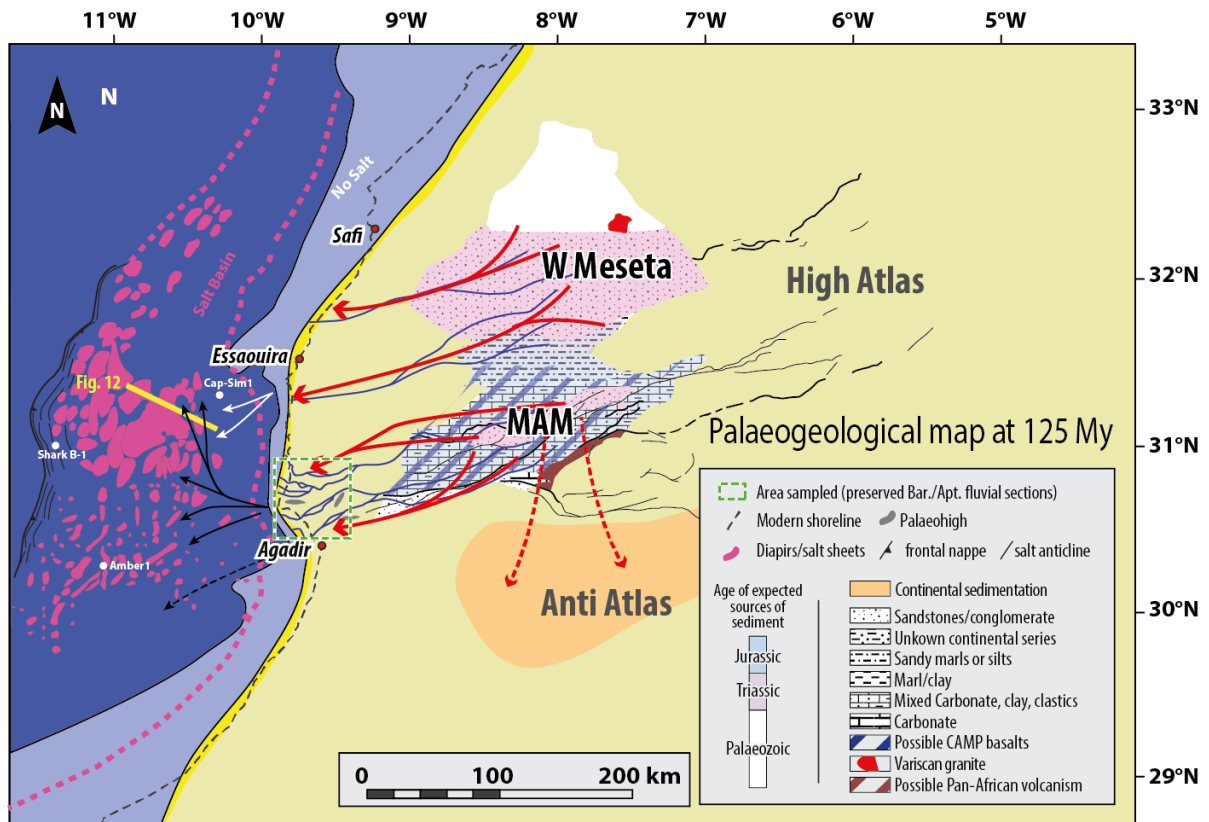

Figure 14: Source-to-sink model of the EAB and surrounding domains during the Barremian-Aptian transition. Onshore drainage marked in red, offshore drainage in black (dashed lines shows lower confidence, see text for details). Location and repartition of exposed lithologies within the MAM are not constrained. Rehamna massif displayed here without overburden (basement exposed) as its presence during the Barremian-Aptian is within error margins. See text for details of transport and exposed lithologies.

1.8 Conclusion

12 outcrops of the Essaouira-Agadir Basin exposing fluvial sandstones of the Barremian-Aptian regression were sampled and analysed. Thin section petrography and SEM, heavy minerals analysis, and detrital zircon dating were conducted and integrated with a large dataset of published low-temperature thermochronology studies to model the associated source-to-sink system. The homogeneity of fingerprints throughout the basin indicated a single provenance for both the northern and southern studied transects. The hinterland analysis based on LTT data revealed that

only the Western Meseta and MAM regions were possible source candidates for the Barremian Aptian. This was confirmed by the strong affinity of the detrital zircon geochronology with the Triassic sediments expected to cover the MAM and parts of the Western Meseta. LTT data revealed that both regions are at the time covered by unpreserved Mesozoic sequences overlaying the Palaeozoic basement. Heavy mineral populations confirmed that sediment sources were of recycled nature and rock fragment populations in the EAB revealed clasts of limestones, sandstones and volcanic nature only matching with the MAM.

Therefore, a source-to-sink system of moderate size (200-300 km long) with an exclusive or dominant source located in the MAM (western High Atlas) provides the best fit explanation matching with each individual dataset. This likely provided a sand-rich mix of sediment resulting from the erosion of Triassic continental basins, with associated clays resulting from the weathering of basalts and Triassic /Jurassic mudstones.

Associated low sea level allowed the direct sediment supply within the slope/offshore domain where seismic imaging suggests the presence of synchronous high reflectivity deep-water channels located in structural lows controlled by diapiric salt movement. While the southern part was not imaged and might have been feeding an early Agadir Canyon, an overall NNW drainage direction is observed offshore the northern part of the basin. The Mesetian domain is likely to be undergoing denudation at the same time and shedding a clastic-rich sediment supply north of the studied region. Due to the offshore NNW deflection of the sediment supply along the northern part of the EAB, mixing between MAM and Mesetian sands is likely offshore Essaouira making the probability of good reservoir sands in the region high.

References

Abati, J., Aghzer, A.M., Gerdes, A., Ennih, N., 2010. Detrital zircon ages of Neoproterozoic sequences of the Moroccan Anti-Atlas belt. Precambrian Res. 181, 115–128. https://doi.org/10.1016/j.precamres.2010.05.018

Accotto, C., Martínez Poyatos, D.J., Azor, A., Talavera, C., Evans, N.J., Jabaloy-Sánchez, A., Azdimousa, A., Tahiri, A., El Hadi, H., 2019. Mixed and recycled detrital zircons in the Paleozoic rocks of the Eastern Moroccan Meseta: Paleogeographic inferences. Lithos 338–339, 73–86. https://doi.org/10.1016/j.lithos.2019.04.011

Adams, A.E., 1979. Sedimentary environments and palaeogeography of the western High Atlas, Morocco, during the Middle and late jurassic. Palaeogeogr. Palaeoclimatol. Palaeoecol. 28, 185–196. https://doi.org/10.1016/0031-0182(79)90118-4

Andersen, T., 2005. Detrital zircons as tracers of sedimentary provenance: Limiting conditions from statistics and numerical simulation. Chem. Geol. 216, 249–270. https://doi.org/10.1016/j.chemgeo.2004.11.013

Andersen, T., Kristoffersen, M., Elburg, M.A., 2016. How far can we trust provenance and crustal evolution information from detrital zircons? A South African case study. Gondwana Res. https://doi.org/10.1016/j.gr.2016.03.003

Aomine, S., Wada, K., 1962. Differential Weathering of Volcanic Ash and Pumice, Resulting in Formation of Hydrated Halloysite. Am. Mineral. 47, 1024–1048.

Avigad, D., Gerdes, A., Morag, N., Bechstädt, T., 2012. Coupled U-Pb-Hf of detrital zircons of Cambrian sandstones from Morocco and Sardinia: Implications for provenance and Precambrian crustal evolution of North Africa. Gondwana Res. 21, 690–703. https://doi.org/10.1016/j.gr.2011.06.005

Azdimousa, A., Jabaloy-Sánchez, A., Talavera, C., Asebriy, L., González-Lodeiro, F., Evans, N.J., 2019. Detrital zircon U-Pb ages in the Rif Belt (northern Morocco): Paleogeographic implications. Gondwana Res. 70, 133–150. https://doi.org/10.1016/j.gr.2018.12.008

Bailey, E.H., Stevens, R.E., 1960. Selective staining of K-feldspar and plagioclase on rock slabs and thin sections. Am. Mineral. 45, 1020–1025.

Balestrieri, M.L., Moratti, G., Bigazzi, G., Algouti, A., 2009. Neogene exhumation of the Marrakech High Atlas (Morocco) recorded by apatite fission-track analysis. Terra Nov. 21, 75–82. https://doi.org/10.1111/j.1365-3121.2008.00857.x

Barbero, L., Jabaloy, A., Gómez-Ortiz, D., Pérez-Peña, J. V., Rodríguez-Peces, M.J., Tejero, R., Estupiñán, J., Azdimousa, A., Vázquez, M., Asebriy, L., 2011. Evidence for surface uplift of the Atlas Mountains and the surrounding peripheral plateaux: Combining apatite fission-track results and geomorphic indicators in the Western Moroccan Meseta (coastal Variscan Paleozoic basement). Tectonophysics 502, 90–104. https://doi.org/10.1016/j.tecto.2010.01.005

Barbero, L., Teixell, A., Arboleya, M.L., del R??o, P., Reiners, P.W., Bougadir, B., 2007. Jurassic-to-present thermal history of the central High Atlas (Morocco) assessed by low-temperature thermochronology. Terra Nov. 19, 58–64. https://doi.org/10.1111/j.1365-3121.2006.00715.x

Beauchamp, J., 1988. Triassic sedimentation and rifting in the High Atlas, in: Triassic-Jurassic Rifting : Continental Breakup and the Origin of the Atlantic Ocean and Passive Margins. pp. 477–497.

Behrens, M., Krumsiek, K., Meyer, D.E., Schäfer, E.A., Siehl, A., Stets, J., Thein, J., Wurster, P., 1978. Sedimentationsabläufe im Atlas-Golf (Kreide Küstenbecken Marokko). Geol. Rundschau 67, 424–453. https://doi.org/10.1007/BF01802799

Bertotti, G., Gouiza, M., 2012. Post-rift vertical movements and horizontal deformations in the eastern margin of the Central Atlantic: Middle Jurassic to Early Cretaceous evolution of Morocco. Int. J. Earth Sci. 101, 2151–2165. https://doi.org/10.1007/s00531-012-0773-4

Boher, M., Abouchami, W., Michard, A., Albarede, F., Arndt, N.T., 1992. Crustal growth in West Africa at 2.1 Ga. J. Geophys. Res. 97, 345–369. https://doi.org/10.1029/91JB01640

Butt, A., 1982. Micropalaeontological bathymetry of the Cretaceous of western Morocco. Palaeogeogr. Palaeoclimatol. Palaeoecol. 37, 235–275.

Charton, R., Bertotti, G., Arantegui, A., Bulot, L., 2018. The Sidi Ifni transect across the rifted margin of Morocco (Central Atlantic): Vertical movements constrained by low-temperature thermochronology. J. African Earth Sci. 141, 22–32. https://doi.org/10.1016/j.jafrearsci.2018.01.006

Charton, R., Bertotti, G., Duval-arnould, A., Storms, J.E.A., Redfern, J., 2020. Low-temperature thermochronology as a control on vertical movements for semi-quantitative Source-to-Sink analysis: A case study for the Permian to Neogene of Morocco and surroundings. Basin Res. https://doi.org/10.1111/bre.12517

Cummings, D.J., 2004. Sedimentology and Stratigraphy of an Ancient Progradational Terrigenous Clastic Shelf Margin, Missisauga Formation (Upper Jurassic-Lower Cretaceous) Offshore Nova Scotia, Canada. University of Ottawa.

DeSilva, N.R., 1999. Sedimentary basins and petroleum systems offshore Newfoundland and Labrador. Pet. Geol. Conf. Proc. 5, 501–515. https://doi.org/10.1144/0050501

Domenech, M., 2015. Rift opening and inversion in the Marrakech High Atlas : Intergrated structural and thermochronologic study.

Domènech, M., Stockli, D.F., Teixell, A., 2018. Detrital zircon U–Pb provenance and palaeogeography of Triassic rift basins in the Marrakech High Atlas. Terra Nov. 30, 310–318. https://doi.org/10.1111/ter.12340

El Houicha, M., Pereira, M.F., Jouhari, A., Gama, C., Ennih, N., Fekkak, A., Ezzouhairi, H., El Attari, A., Silva, J.B., 2018. Recycling of the Proterozoic crystalline basement in the Coastal Block (Moroccan Meseta): New insights for understanding the geodynamic evolution of the northern peri-Gondwanan realm. Precambrian Res. 306, 129–154. https://doi.org/10.1016/j.precamres.2017.12.039

Espejo, I.S., Lopez-Gamundi, O.R., 1994. Source versus depositional controls on sandstone composition in a foreland basin: the El Imperial formation (mid carboniferous-lower permian), San Rafael Basin, Western Argentina. J. Sediment. Res. A64, 8–16.

Fabuel-Perez, I., Hodgetts, D., Redfern, J., 2009. A new approach for outcrop characterization and geostatistical analysis of a low-sinuosity fluvial-dominated succession using digital outcrop models: Upper triassic oukaimeden sandstone formation, central high Atlas, Morocco. Am. Assoc. Pet. Geol. Bull. 93, 795–827. https://doi.org/10.1306/02230908102

Frizon de Lamotte, D., Zizi, M., Missenard, Y., Hafid, M., El Azzouzi, M., Maury, R., Charriere, A., Taki, Z., Benammi, M., Michard, A., 2008. The Atlas System, in: Continental Evolution: The Geology of Morocco: Structure, Stratigraphy, and Tectonics of the Africa-Atlantic-Mediterranean Triple Junction. p. 133.

Gallagher, K., Brown, R., Johnson, C., 1998. Fission Track Analysis and Its Applications To Geological Problems. Annu. Rev. Earth Planet. Sci. 26, 519–572. https://doi.org/10.1146/annurev.earth.26.1.519

Gärtner, A., Youbi, N., Villeneuve, M., Linnemann, U., Sagawe, A., Hofmann, M., Zieger, J., Mahmoudi, A., Boumehdi, M.A., 2018. Provenance of detrital zircon from siliciclastic rocks of the Sebkha Gezmayet unit of the Adrar Souttouf Massif (Moroccan Sahara) – Palaeogeographic implications. Comptes Rendus - Geosci. 350, 255–266. https://doi.org/10.1016/j.crte.2018.06.004

Gärtner, A., Youbi, N., Villeneuve, M., Sagawe, A., Hofmann, M., Mahmoudi, A., Boumehdi, M.A., Linnemann, U., 2017. The zircon evidence of temporally changing sediment transport—the NW Gondwana margin during Cambrian to Devonian time (Aoucert and Smara areas, Moroccan Sahara). Int. J. Earth Sci. (Geol Rundsch) 1–23. https://doi.org/10.1007/s00531-017-1457-x

Garzanti, E., 2019. Petrographic classification of sand and sandstone. Earth-Science Rev. 192, 545–563. https://doi.org/10.1016/j.earscirev.2018.12.014

Garzanti, E., Andò, S., 2007. Chapter 20 Heavy Mineral Concentration in Modern Sands: Implications for Provenance Interpretation. Dev. Sedimentol. 58, 517–545. https://doi.org/10.1016/S0070-4571(07)58020-9

Gasquet, D., Ennih, N., Liégeois, J.-P., Soulaimani, A., Michard, A., 2008. The pan-African belt. Lect. Notes Earth Sci. 116, 33–64. https://doi.org/10.1007/978-3-540-77076-3_2

Ghienne, J.F., Benvenuti, A., El Houicha, M., Girard, F., Kali, E., Khoukhi, Y., Langbour, C., Magna, T., Míková, J., Moscariello, A., Schulmann, K., 2018. The impact of the end-Ordovician glaciation on sediment routing systems: A case study from the Meseta (northern Morocco). Gondwana Res. 63, 169–178. https://doi.org/10.1016/j.gr.2018.07.001

Ghorbal, B., 2009. Mesozoic to Quaternary thermotectonic evolution of Morocco (NW Africa). Vrije Universiteit Amsterdam.

Ghorbal, B., Bertotti, G., Foeken, J., Andriessen, P., 2008. Unexpected Jurassic to Neogene vertical movements in 'stable'parts of NW Africa revealed by low temperature geochronology. Terra Nov. 20, 355–363. https://doi.org/10.1111/j.1365-3121.2008.00828.x

Gouiza, M., Charton, R., Bertotti, G., Andriessen, P., Storms, J.E.A., 2017. Post-Variscan evolution of the Anti-Atlas belt of Morocco constrained from low-temperature geochronology. Int. J. Earth Sci. 106, 593–616. https://doi.org/10.1007/s00531-016-1325-0

Guedes, C.C.F., Giannini, P.C.F., Nascimento, D.R., Sawakuchi, A.O., Tanaka, A.P.B., Rossi, M.G., 2011. Controls of heavy minerals and grain size in a holocene regressive barrier (Ilha Comprida, southeastern Brazil). J. South Am. Earth Sci. 31, 110–123. https://doi.org/10.1016/j.jsames.2010.07.007

Hafid, M., Zizi, M., Bally, A.W., Ait Salem, A., 2006. Structural styles of the western onshore and offshore termination of the High Atlas, Morocco. Comptes Rendus - Geosci. 338, 50–64. https://doi.org/10.1016/j.crte.2005.10.007

Hoepffner, C., Houari, M.R., Bouabdelli, M., 2006. Tectonics of the North African Variscides (Morocco, western Algeria): an outline. Comptes Rendus Geosci. 338, 25–40. https://doi.org/10.1016/J.CRTE.2005.11.003

Hoepffner, C., Soulaimani, A., Piqué, A., 2005. The Moroccan Hercynides. J. African Earth Sci. 43, 144–165. https://doi.org/10.1016/j.jafrearsci.2005.09.002

Hubert, J.F., 1962. A Zircon-Tourmaline-Rutile Maturity Index and the Interdependence of the Composition of Heavy Mineral Assemblages with the Gross Composition and Texture of Sandstones. SEPM J. Sediment. Res. Vol. 32, 440–450. https://doi.org/10.1306/74d70ce5-2b21-11d7-8648000102c1865d

Ingersoll, R. V., Bullard, T.F., Ford, R.L., Grimm, J.P., Pickle, J.D., Sares, S.W., 1984. The effect of grain size on detrital modes: a test of the Gazzi- Dickinson point-counting method (Holocene, sand, New Mexico, USA). J. Sediment. Petrol. 54, 103–116.

Le Roy, P., Piqué, A., 2001. Triassic-Liassic western Moroccan synrift basins in relation to the Central Atlantic opening. Mar. Geol. 172, 359–381. https://doi.org/10.1016/S0025-3227(00)00130-4

Leprêtre, R., 2015. Evolution phanérozoïque du Craton Ouest Africain et de ses bordures Nord et Ouest. Université Paris Sud - Paris XI.

Luber, T.L., 2017. Integrated analysis of Lower Cretaceous stratigraphy and depositional systems : the Essaouira-Agadir basin of Morocco.

Luber, T.L., Bulot, L.G., Redfern, J., Frau, C., Arantegui, A., Masrour, M., 2017. A revised ammonoid biostratigraphy for the Aptian of NW Africa: Essaouira-Agadir Basin, Morocco. Cretac. Res. 79, 12–34. https://doi.org/10.1016/j.cretres.2017.06.020

Luber, T.L., Bulot, L.G., Redfern, J., Nahim, M., Jeremiah, J., Simmons, M., Bodin, S., Frau, C., Bidgood, M., Masrour, M., 2019. A revised chronostratigraphic framework for the Aptian of the Essaouira-Agadir Basin, a candidate type section for the NW African Atlantic Margin. Cretac. Res. 93, 292–317. https://doi.org/10.1016/j.cretres.2018.09.007

Mader, N.K., Redfern, J., El Ouataoui, M., 2017. Sedimentology of the Essaouira Basin (Meskala Field) in context of regional sediment distribution patterns during upper Triassic pluvial events. J. African Earth Sci. 130, 293–318. https://doi.org/10.1016/j.jafrearsci.2017.02.012

Malusà, M.G., Polino, R., Feroni, A.C., Ellero, A., Ottria, G., Baidder, L., Musumeci, G., 2007. Post-Variscan tectonics in eastern anti-atlas (Morocco). Terra Nov. 19, 481–489. https://doi.org/10.1111/j.1365-3121.2007.00775.x

Marzoli, A., Bertrand, H., Youbi, N., Callegaro, S., Merle, R., Reisberg, L., Chiaradia, M., Brownlee, S.I., Jourdan, F., Zanetti, A., Davies, J.H.F.L., Cuppone, T., Mahmoudi, A., Medina, F., Renne, P.R., Bellieni, G., Crivellari, S., El Hachimi, H., Bensalah, M.K., Meyzen, C.M., Tegner, C., 2019. The Central Atlantic Magmatic Province (CAMP) in Morocco. J. Petrol. 60, 945–996. https://doi.org/10.1093/petrology/egz021

Marzoli, A., Davies, J.H.F.L., Youbi, N., Merle, R., Corso, J.D., Dunkley, D.J., Fioretti, A.M., Bellieni, G., Medina, F., Wotzlaw, J.-F., McHone, G., Font, E., Bensalah, M.K., 2017. Proterozoic to Mesozoic evolution of North-West Africa and Peri-Gondwana microplates: Detrital zircon ages from Morocco and Canada. Lithos 278–281, 229–239. https://doi.org/10.1016/j.lithos.2017.01.016

Medina, F., 1995. Syn- and postrift evolution of the El Jadida – Agadir basin (Morocco): constraints for the rifting models of the central Atlantic. Can. J. Earth Sci. 32, 1273–1291. https://doi.org/10.1139/e95-104

Medina, F., 1991. Superimposed extensional tectonics in the Argana Triassic formations (Morocco), related to the early rifting of the Central Atlantic. Geol. Mag. 128, 525–536. https://doi.org/10.1017/S0016756800018665

Michard, A., Hoepffner, C., Soulaimani, A., Baidder, L., 2008. The Variscan Belt. Cont. Evol. Geol. Morocco 65–132. https://doi.org/10.1007/978-3-540-77076-3_3

Morton, A.C., 2012. Value of heavy minerals in sediments and sedimentary rocks for provenance, transport history and stratigraphic correlation, in: Quantitative Mineralogy and Microanalysis of Sediments and Sedimentary Rocks: Mineralogical Association of Canada Short Course. pp. 133–165.

Morton, A.C., 1984. Stability of detrital heavy tertiary sandstones from sea basin minerals in the north. Clay Miner. 19, 287–308. https://doi.org/10.1180/claymin.1984.019.3.04

Mrini, Z., Rafi, A., Duthou, J.-L., Vidal, P., 1992. Chronologie Rb-Sr des granitoides hercyniens du Maroc : conséquences. Bull. la Soc. Geol. Fr. 163, 281–291.

Neumaier, M., 2015. Structural Restoration and Basin and Petroleum Systems Modeling : Case Studies from the Monagas Fold and Thrust Belt , Venezuela and the Moroccan Atlantic Margin Von der Fakultät für Georessourcen und Materialtechnik der Rheinisch -Westfälischen Technisch.

Nouidar, M., Chellai, E.H., 2000. Facies and sequence stratigraphy of Upper Barremian-Lower Aptian Bouzergoun Formation, Agadir basin, Morocco. Africa Geosci. Rev. 7, 327–340. https://doi.org/http://dx.doi.org/10.1006/cres.2000.0239

Oukassou, M., Saddiqi, O., Barbarand, J., Sebti, S., Baidder, L., Michard, A., 2013. Post-Variscan exhumation of the Central Anti-Atlas (Morocco) constrained by zircon and apatite fission-track thermochronology. Terra Nov. 25, 151–159. https://doi.org/10.1111/ter.12019

Paton, C., Hellstrom, J., Paul, B., Woodhead, J., Hergt, J., 2011. Iolite: Freeware for the visualisation and processing of mass spectrometric data. J. Anal. At. Spectrom. 26, 2508–2518. https://doi.org/10.1039/c1ja10172b

Paton, C., Woodhead, J.D., Hellstrom, J.C., Hergt, J.M., Greig, A., Maas, R., 2010. Improved laser ablation U-Pb zircon geochronology through robust downhole fractionation correction. Geochemistry, Geophys. Geosystems 11. https://doi.org/10.1029/2009GC002618

Perez, N.D., Teixell, A., Gómez-Gras, D., Stockli, D.F., 2019. Reconstructing Extensional Basin Architecture and Provenance in the Marrakech High Atlas of Morocco: Implications for Rift Basins and Inversion Tectonics. Tectonics 38, 1584–1608. https://doi.org/10.1029/2018TC005413

Pichel, L.M., Huuse, M., Redfern, J., Finch, E., 2019. The influence of base-salt relief, rift topography and regional events on salt tectonics offshore Morocco. Mar. Pet. Geol. 103, 87–113. https://doi.org/10.1016/j.marpetgeo.2019.02.007

Potrel, A., Peucat, J.-J., Fanning, M., Auvray, B., Burg, J.., Caruba, C., 2007. 3.5 Ga old terranes in the West African Craton, Mauritania. J. Geol. Soc. London. https://doi.org/10.1144/gsjgs.153.4.0507

Rey, J., Canerot, J., Peybernes, B., Taj-Eddine, K., Rahhali, K., Thieuloy, J.P., 1986. Le Crétacé inférieur de la région d'Essaouira : données biostratigraphiques et évolutions. Rev. la Fac. des Sci. marrakech no spécial, 413–441.

Rey, J., Canérot, J., Peybernès, B., Taj-Eddine, K., Thieuloy, J.P., 1988. Lithostratigraphy, biostratigraphy and sedimentary dynamics of the Lower Cretaceous deposits on the northern side of the western High Atlas (Morocco). Cretac. Res. 9, 141–158. https://doi.org/10.1016/0195-6671(88)90014-6

Ruiz, G.M.H., Sebti, S., Negro, F., Saddiqi, O., Frizon de Lamotte, D., Stockli, D., Foeken, J., Stuart, F., Barbarand, J., Schaer, J.P., 2011. From central Atlantic continental rift to Neogene uplift - western Anti-Atlas (Morocco). Terra Nov. 23, 35–41. https://doi.org/10.1111/j.1365-3121.2010.00980.x

Sabil, N., 1995. La datation par traces de fission: aspects méthodologiques et applications thermochronologiques en contexte alpin et de marge continentale 238.

Saddiqi, O., El Haimer, F.Z., Michard, A., Barbarand, J., Ruiz, G.M.H., Mansour, E.M., Leturmy, P., Frizon de Lamotte, D., 2009. Apatite fission-track analyses on basement granites from south-western Meseta, Morocco: Paleogeographic implications and interpretation of AFT age discrepancies. Tectonophysics 475, 29–37. https://doi.org/10.1016/j.tecto.2009.01.007

Sahabi, M., Aslanian, D., Olivet, J.-L., 2004. Un nouveau point de départ pour l'histoire de l'Atlantique central. Comptes Rendus Geosci. 336, 1041–1052.

Schlische, R.W., Withjack, M.O., Olsen, P.E., 2013. Relative Timing of CAMP, Rifting, Continental Breakup, and Basin Inversion: Tectonic Significance. Cent. Atl. Magmat. Prov. Insights from Fragm. Pangea 33–59. https://doi.org/10.1029/136GM03

Scotese, C.R., 2016. PALEOMAP PaleoAtlas for GPlates and the PaleoData Plotter Program [WWW Document]. PALEOMAP Proj.

Sebti, S., 2011. Mouvements verticaux de l'Anti-Atlas occidental marocain (Kerdous & Ifni): Thermochronologie par traces de fission. Université Hassan II.

Sebti, S., Saddiqi, O., El Haimer, F.Z., Michard, A., Ruiz, G., Bousquet, R., Baidder, L., Frizon de Lamotte, D., 2009. Vertical movements at the fringe of the West African Craton: First zircon fission track datings from

the Anti-Atlas Precambrian basement, Morocco. Comptes Rendus - Geosci. 341, 71–77. https://doi.org/10.1016/j.crte.2008.11.006

Sehrt, M., 2014. Variscan to neogene long-term landscap eevolution at the Moroccan passive continental margin (Tarfaya Basin and western anti-Atlas). Ph.D Thesis, Heidelb.

Sláma, J., Košler, J., Condon, D.J., Crowley, J.L., Gerdes, A., Hanchar, J.M., Horstwood, M.S.A., Morris, G.A., Nasdala, L., Norberg, N., Schaltegger, U., Schoene, B., Tubrett, M.N., Whitehouse, M.J., 2008. Plešovice zircon - A new natural reference material for U-Pb and Hf isotopic microanalysis. Chem. Geol. 249, 1–35. https://doi.org/10.1016/j.chemgeo.2007.11.005

Soulaimani, A., Ouanaimi, H., Saddiqi, O., Baidder, L., Michard, A., 2018. The Anti-Atlas Pan-African Belt (Morocco): Overview and pending questions. Comptes Rendus - Geosci. https://doi.org/10.1016/j.crte.2018.07.002

Stephan, T., Kroner, U., Romer, R.L., 2019. The pre-orogenic detrital zircon record of the Peri-Gondwanan crust. Geol. Mag. 156, 281–307. https://doi.org/10.1017/S0016756818000031

Sudo, T., 1954. Clay mineralogical aspects of alteration of volcanic glass in Japan. Clay Miner. Bull. 2, 96–105.

Tari, G., Jabour, H., Tari, G., Jabour, H., 2014. Salt tectonics along the Atlantic margin of Morocco Salt tectonics along the Atlantic margin of Morocco. Conjug. Divergent Margins. 337–353. https://doi.org/10.1144/SP369.23

Ulmer-Scholle, D.S., Scholle, P.A., Schieber, J., Raine, R.J., 2015. A Color Guide to the Petrography of Sandstones, Siltstones, Shales and Associated Rocks. American Association of Petroleum Geologists.

Vermeesch, P., 2018. IsoplotR: A free and open toolbox for geochronology. Geosci. Front. 9, 1479–1493. https://doi.org/10.1016/j.gsf.2018.04.001

Wiedenbeck, M., Allé, P., Corfu, F., Griffin, W.L., Meier, M., Oberli, F., Quadt, A. VON, Roddick, J.C., Spiegel, W., 1995. Three Natural Zircon Standards for U-Th-Pb, Lu-Hf, Trace Element and Ree Analyses. Geostand. Newsl. 19, 1–23. https://doi.org/10.1111/j.1751-908X.1995.tb00147.x

Wiedmann, J., Butt, A., Einsele, G., 1978. Vergleich von marokkanischen Kreide-Küstenaufschlüssen und Tiefseebohrungen (DSDP): Stratigraphie, Paläoenvironment und Subsidenz an einem passiven Kontinentalrand. Geol. Rundschau 67, 454–508. https://doi.org/10.1007/BF01802800

Wipf, M., Glasmacher, U.A., Stockli, D.F., Emmerich, A., Bechstädt, T., Baur, H., 2010. Reconstruction of the differentiated long-term exhumation history of Fuerteventura, Canary Islands, Spain, through fission-track and (U-Th-Sm)/He data. Int. J. Earth Sci. 99, 675–686. https://doi.org/10.1007/s00531-008-0415-z

1.9 Appendix

Region	Low-temperature thermochronology time-temperature models
Western Anti-Atlas	(Charton et al., 2018; Gouiza et al., 2017; Leprêtre, 2015; Ruiz et al., 2011; Sebti, 2011; Sehrt, 2014)
Central Anti-Atlas	(Balestrieri et al., 2009; Ghorbal, 2009; Gouiza et al., 2017; Oukassou et al., 2013)
Eastern Anti-Atlas	(Barbero et al., 2007; Gouiza et al., 2017; Malusà et al., 2007)
MAM/High Atlas	(Balestrieri et al., 2009; Barbero et al., 2007; Domenech, 2015; Ghorbal, 2009)
Western Meseta	(Ghorbal, 2009; Ghorbal et al., 2008; Sabil, 1995; Saddiqi et al., 2009; Sebti et al., 2009)

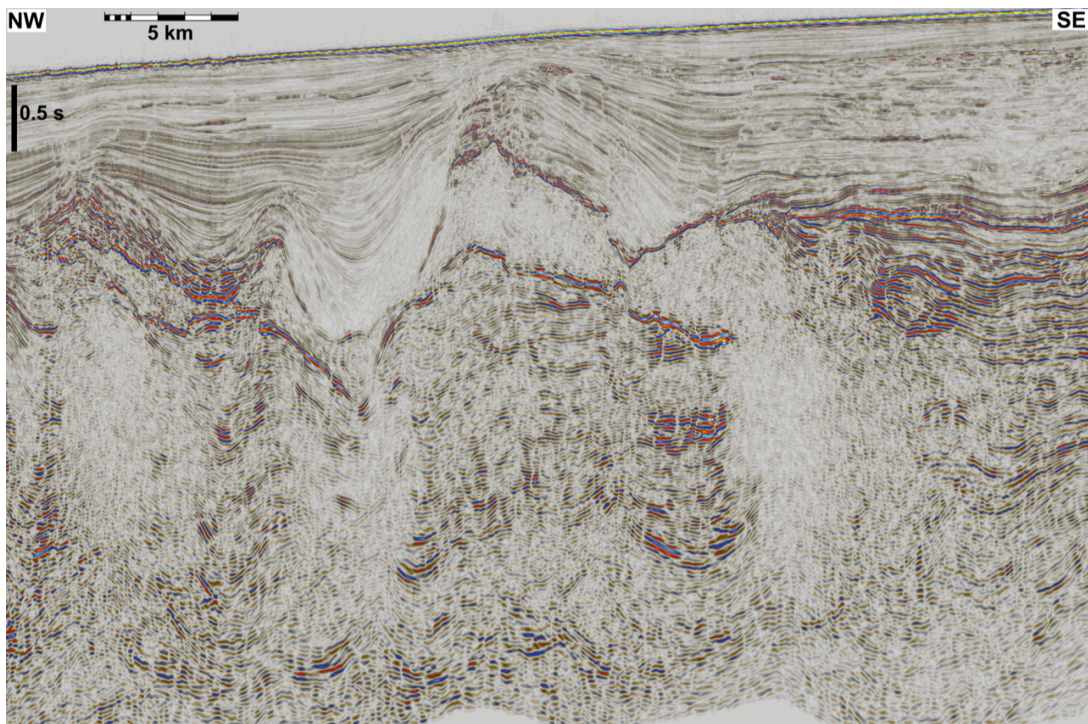**Table A1: Reference of LTT datasets used to constrain burial and exhumation patterns on Figure 7.**

Figure A: Uninterpreted seismic line offshore Assaka presented in Figure 12

Outcrop name	Outcrop code	Latitude	Longitude
Tiskatine North	MTTN	30,84342	-9,67121
Assaka	MTAS	30,81406	-9,77168
Aziar North	MTAZ	30,80863	-9,61164
Aziar	MTDAN	30,76080	-9,58976
West Barrage / Akerkaou	MTWB	30,75538	-9,75881
Barrage	MTBR	30,75895	-9,68653
Tinkert	MTTK	30,73577	-9,63322
Mahmout	MTMH	30,72021	-9,80223
Tamri	MTTM	30,70460	-9,82758
Addar	MTAD	30,60226	-9,71919
Aouerga	MTAO	30,59358	-9,64122
Tamzergout	MTTZ	30.55127	-9.55678

Table A2: Outcrop coordinates and code name